FIELD AND LABORATORY EXPERIMENT TO ESTIMATE BULKING FACTOR FOR A LITHOPHYSAL TUFF, FRAN RIDGE, YUCCA MOUNTAIN, NEVADA

Prepared for

U.S. Nuclear Regulatory Commission
Contract NRC–02–07–006

Prepared by

Danielle Wyrick[1]
Randall Fedors[3]
Kevin Smart[1]
Robert Lenhard[2]
Ronald McGinnis[1]
Donald Bannon[2]
Chandrika Manepally

[1]Department of Earth, Material, and Planetary Sciences
San Antonio, Texas

[2]Center for Nuclear Waste Regulatory Analyses
San Antonio, Texas

[3]U.S. Nuclear Regulatory Commission
Washington DC

September 2011

ABSTRACT

This report presents the results of field work and laboratory testing to estimate the bulking factor for the Topopah Springs welded lower lithophysal tuff, Yucca Mountain, Nevada. Bulking factor is used in performance assessment analyses to constrain the amount of rubble spalling from the drift ceiling and covering the drip shield. The field and laboratory testing utilized data and rock taken from an analog site for the drift environment. The field site was a surface exposure of the lower lithophysal unit on the south end of Fran Ridge, which is a small ridge east of Yucca Mountain. Rock fragments from several outcrops were collected, shipped to the laboratory, and repacked using several approaches to obtain estimates of rubble bulk density, which leads directly to estimates of bulking factor. The dominant shape of fragments could be described as bladed and elongated. Bulking factors estimated from these experiments range from 1.62 to 1.83. Collection and analysis of fracture and fragment shape data from the analog site could facilitate both the correlation of experiment data with the range of fracturing along drifts, and estimation of permeability and thermal conductivity of rubble needed for modeling thermohydrological conditions. The approaches used for laboratory repacking of the rock fragments illustrate different extents of packing, but these approaches may not directly be correlated with the physical effects of static loads or shaking due to earthquakes as expected over long time periods in drifts. Thus, these estimates of bulking factor reported herein likely reflect early values of bulking factor or reflect the upper portion of the range of long-term bulking factors expected in drifts.

CONTENTS

Section Page

ABSTRACT ii
FIGURES iv
TABLES vi
ACKNOWLEDGMENTS vii

1 INTRODUCTION 1-1

2 FIELD EXPERIMENT 2-1
2.1 Field Investigation 2-1
2.2 Fracture Characterization 2-3
2.3 Rubble Characterization 2-5
2.3.1 Clast Shape Distribution 2-5
2.3.2 Clast Size Distribution 2-22

3 LABORATORY MEASUREMENT OF BULKING FACTOR 3-1
3.1 Introduction 3-1
3.2 Bulk Density of Rubble 3-1

4 SUMMARY 4-1

5 REFERENCES 5-1

FIGURES

Figure Page

2-1 A Location Map of Fran Ridge Outcrop Sites Inset Shows Location With Respect to the Exploratory Studies Facility (ESF) at Yucca Mountain 2-2
2-2 Example Rubble Pile Collected From Plot 2 Outcrop at Fran Ridge 2-3
2-3 Examples of Basic Rubble Shapes. (A) Platy, (B) Cubic, (C) Bladed, and (D) Elongate 2-4
2-4 Equal-Area Stereonet Plot of Poles to Fracture Planes From Fracture Orientation Data Collected at Fran Ridge Outcrop (Green Circles) and the ESF/ECRB Detailed Line Survey Small-Scale Fracture Data 2-6
2-5 Equal-Area Stereonet Plot of Poles to the Mean Fracture Set Planes 2-6
2-6 A Modified Sneed and Folk Diagram Representation of Particle Shape 2-8
2-7 Modified Sneed and Folk Diagram of All Rubble Shape Data 2-9
2-8 Rubble Shape Major Classification by Percentage for All Rubble Shape Data 2-9
2-9 Rubble Shape Major Classification by Percentage for All Rubble Shape Data 2-10
2-10 Rubble Shape Classification Detailed by Percentage for All Rubble Shape Data 2-10
2-11 Field Photograph of Talus Pile Location for Plot 1A 2-11
2-12 Modified Sneed and Folk Diagram of Plot 1A Rubble Shape Data 2-11
2-13 Rubble Shape Major Classification by Percentage for Plot 1A Rubble Shape Data 2-12
2-14 Rubble Shape Major Classification by Percentage for Plot 1A Rubble Shape Data 2-12
2-15 Rubble Shape Classification Detail by Percentage for Plot 1A Rubble Shape Data 2-13
2-16 Field Photograph of Rubble Collection Area Plot 2 2-13
2-17 Modified Sneed and Folk Diagram of Plot 2A Rubble Shape Data 2-14
2-18 Rubble Shape Major Classification by Percentage for Plot 2A Rubble Shape Data 2-14
2-19 Rubble Shape Major Classification by Percentage for Plot 2A Rubble Shape Data 2-15
2-20 Rubble Shape Classification Detail by Percentage for Plot 2A Rubble Shape Data 2-15
2-21 Modified Sneed and Folk Diagram of Plot 2B Rubble Shape Data 2-16
2-22 Rubble Shape Major Classification by Percentage for Plot 2B Shape Data 2-16
2-23 Rubble Shape Major Classification by Percentage for Plot 2B Rubble Shape Data 2-17
2-24 Rubble Shape Classification Detail by Percentage for Plot 2B Rubble Shape Data 2-17
2-25 Modified Sneed and Folk Diagram of Plot 2C Rubble Shape Data 2-18
2-26 Rubble Shape Major Classification by Percentage for Plot 2C Rubble Shape Data 2-18
2-27 Rubble Shape Major Classification by Percentage for Plot 2C Rubble Shape Data 2-19
2-28 Rubble Shape Classification Detail by Percentage for Plot 2C Rubble Shape Data 2-19
2-29 Field Photograph of Talus Pile Location for Plot 3 2-20
2-30 Modified Sneed and Folk Diagram of Plot 3 Rubble Shape Data 2-20
2-31 Rubble Shape Major Classification by Percentage for Plot 3 Rubble Shape Data 2-21
2-32 Rubble Shape Major Classification by Percentage for Plot 3 Rubble Shape Data 2-21
2-33 Rubble Shape Classification Detail by Percentage for Plot 3 Rubble Shape Data 2-22
2-34 Frequency of Length (Longest Orthogonal Dimension) Measurements 2-23
2-35 Cumulative Frequency Distribution Plot of Rubble Clast Length, Width, and Height From All Plots 2-23
2-36 Frequency of Clast Volume. Note That Volume Measurements Are Truncated at 4,000 cm^3 [244.09 in^3] To Illustrate Smaller Values 2-24
2-37 Cumulative Frequency Distribution Plot of Rubble Clast Volume From All Plots 2-24
2-38 Plot of (Length/Width) Versus (Width/Height) Illustrates the Limited Binning Effect Described on Size Distributions. 2-25
2-39 Cumulative Frequency Distribution Plot of Rubble Clast Volume From Plot 1 2-25

FIGURES (continued)

Figure Page

2-40 Cumulative Frequency Distribution Plot of Rubble Clast Length, Width, and Height From Plot 1 2-26
2-41 Cumulative Frequency Distribution Plot of Rubble Clast Volume From Plot 2A 2-26
2-42 Cumulative Frequency Distribution Plot of Rubble Clast, Length, Width, and Height From Plot 2A 2-27
2-43 Cumulative Frequency Distribution Plot or Rubble Clast Volume From Plot 2B 2-27
2-44 Cumulative Frequency Distribution Plot of Rubble Clast Length, Width, and Height From Plot 2B 2-28
2-45 Cumulative Frequency Distribution Plot of Rubble Clast Volume From Plot 2C 2-28
2-46 Cumulative Frequency Distribution Plot of Rubble Clast Length, Width, and Height From Plot 2C 2-29
2-47 Cumulative Frequency Distribution Plot of Rubble Clast Volume From Plot 3 2-29
2-48 Cumulative Frequency Distribution Plot or Rubble Clast Length, Width, and Height From Plot 3 2-30

3-1 Experimental Setup To Determine Mass Density of Packed Rubble (A) Container 1—Cubic Shape, (B) Top View of Container 1, and (C) Container 2—Rectangular Shape 3-3

TABLES

Table Page

2-1 Summary of Fran Ridge Fracture Data Collected at All Plots 2-4
2-2 Summary of Fran Ridge Fracture Data Collected at Plot 1 2-7
2-3 Summary of Fran Ridge Fracture Data Collected at Plot 2 2-7
2-4 Summary of Fran Ridge Fracture Data Collected at Plot 3 2-7

3-1 Bulk Density of Rubble From Laboratory Measurements Assuming *In-Situ* (Intact) Bulk Density of 1,979 kg/m^3 3-4

ACKNOWLEDGMENTS

This report describes work performed by the Center for Nuclear Waste Regulatory Analyses (CNWRA®) and its contractors for the U.S. Nuclear Regulatory Commission (USNRC) under Contract No. NRC–02–07–006. The activities reported here were performed on behalf of the USNRC Office of Nuclear Material Safety and Safeguards, Division of High-Level Waste Repository Safety and Safeguards, Division of High-Level Waste Repository Safety. This report is an independent product of the CNWRA and does not necessarily reflect the view or regulatory position of the USNRC. The USNRC staff views expressed herein are preliminary and do not constitute a final judgment or determination of the matters addressed or of the acceptability of any licensing action that may be under consideration at USNRC.

The authors gratefully acknowledge A. Morris for his technical review, E. Pearcy for his programmatic review, L. Mulverhill for her editorial review, and A. Ramos for his administrative support.

QUALITY OF DATA, ANALYSES, AND CODE DEVELOPMENT

DATA: All CNWRA-generated original data contained in this report meet quality assurance requirements described in the Geosciences and Engineering Division Quality Assurance Manual. Sources of other data should be consulted for determining the level of quality of those data. The work presented in this report is documented in Scientific Notebook Nos. 852 and 779E (Wyrick, 2011; Bannon, 2006).

ANALYSES AND CODES: Microsoft® Excel® 2003 (Microsoft Corporation, Inc., 2003) and RockWare StereoStat® Version 1.4 (Rockware, Inc. 2004).

REFERENCES

Bannon, D. "Rubble Flow Laboratory Experiment." Scientific Notebook 779E. San Antonio, Texas: CNWRA. 2006.

Microsoft Corporation, Inc. "Microsoft Excel 2003." Redmond, Washington: Microsoft Corporation. 2003.

Rockware, Inc. "StereoStat Version 1.4." Golden, Colorado: Rockware, Inc. 2004.

Wyrick, D. "Fran Ridge Topopah Springs Welded (TSw) Lower Lithophysal Unit Rubble Characterization." Scientific Notebook 852. San Antonio, Texas: CNWRA. 2011.

1 INTRODUCTION

Field and laboratory experiments were performed to help understand the nature of rockfall that may form a rubble pile on top of and to the sides of drip shields in emplacement drifts of a proposed high-level waste repository at Yucca Mountain. The nature and characteristics of rubble that may result from degradation of emplacement drifts in welded lithophysal rocks have not been previously determined. Spalling of rock during the drift-scale heater test and fragments found in the invert in the Exploratory Studies Facility tunnel and enhanced characterization of repository block cross-drift provide qualitative information on the size and shape of fragments. More detailed and quantitative information on rubble characteristics, however, is not available at these locations.

The field and laboratory work focused on estimation of a bulking factor, which is related to the rubble bulk density, and characterized fracture and fragment shape and size information. An understanding of the fragment sizes and shapes and their packing could help constrain estimates of the bulking factor, which constrains the extent (or thickness) of rubble that may occur above drip shields and waste packages. In addition, the size and shape distributions of the fragments and their packing in rubble piles are needed to conceptualize and quantify the flow of water (liquid and gas phase) and heat transfer (conduction, convection, and radiation) for determining the evolution of in-drift environments used in performance assessments of a potential repository (e.g., Mohanty, et al., 2006).

Surface exposure of the Topopah Spring welded lower lithophysal zone at the south end of Fran Ridge, Yucca Mountain, were identified as an analog site to the host rock that would enable detailed fracture characterization and collection of rubble samples (Smart and Fedors, 2006). Field work was performed to characterize surface exposures of the Topopah Springs welded lower lithophysal tuff (Tptpll)[1] zone on the southern end of Fran Ridge (Wyrick, et al., 2007). The supposition is that fracture orientation and spacing control the size and shape of rock blocks that can form, which in turn influence the assessments of the distribution and size of rubble piles that accumulate on waste packages from rock fall (Smart, et al., 2006). The objective of the field work was to obtain a more quantitative understanding of rubble size distributions by examining fractured outcrops of lower lithophysal rock and nearby talus piles on the southern end of Fran Ridge. Degradation in emplacement drifts and the resulting block size and bulking factor are influenced by existing fractures. The surface exposures and talus, therefore, may provide a link between fracture patterns and rubble fragment size and shape distributions that would be useful for understanding drift degradation and the extent of spallation in drift ceilings. The effect of surficial processes on fracture and fragment characteristics is acknowledged, but neglected, in this study.

Section 2 of this report describes a focused investigation on the size and shape distributions of rubble resulting from fractured lower lithophysal rock, which, along with detailed fracture data collection, provided an outcrop-scale rubble characterization for subsequent modeling efforts. Section 3 describes laboratory experiments using different packing approaches to estimate a range of bulking factors for rubble.

[1]Topopah Spring welded Lower Lithophysal zone is used frequently throughout this chapter; therefore, the acronym Tptpll will be used.

2 FIELD EXPERIMENT

Staff made two field excursions to Yucca Mountain as part of an effort to quantify bulking factor for a welded lithophysal tuff. The first excursion (Smart and Fedors, 2006) focused on familiarization with and visits to surface and subsurface exposures of the Tptpll. During this excursion, it was determined that the Topopah Springs welded upper lithophysal zone would not serve as a reasonable analog, because of the different character of fracturing compared to that of the lower lithophysal unit. The identified analog site at the south end of Fran Ridge exhibited a range of fracture densities, due in part to the close proximity to a mapped fault. The second excursion focused on excavation and characterization of the selected rubble analog site (Wyrick, et al., 2007).

This section of the report documents the (i) site description, excavation of several plots at three intact outcrops, and collection of rubble; (ii) characterization of fracture patterns and density in the vicinity of each plot; and (iii) shape and size characterization of rubble fragments in the last subsection.

2.1 Field Investigation

The south end of Fran Ridge at Yucca Mountain has outcrop exposures of the Tptpll that are easily accessible (Figure 2-1) because of close proximity to a road. Three outcrop areas were delineated in the field, designated as Plot 1, Plot 2, and Plot 3. Plot 2 was further subdivided for rubble collection and characterization into subareas A, B, and C. Fracture data were collected from the three field outcrops. Data collection included fracture orientation, spacings, and tracelength (where it could be determined). Fracture orientation data were collected as strike, dip, and dip direction. Values were then converted to right-hand rule azimuth direction for subsequent analyses.

There were two methods of rubble collection. For the first method, talus was collected from immediately beneath outcrops for Plots 1 and 3. Upslope characteristics supported the observation that the rubble fragments could only have come from the identified outcrop and could not have been transported from adjacent areas (e.g., transported down slope from above the outcrop area). Known limitations to the field data at Plots 1 and 3 include secondary alteration to the rubble (e.g., weathering and erosion effects). The smallest material in the talus piles of Plots 1 and 3 (i.e., fine-grained particles) was not included in the collection or analysis, because it was not possible to distinguish particles that originated from the outcrop from those introduced by eolian transport or other means. The second method of rubble collection minimized the uncertainty of origin for the fine particles. Rock fragments from Plot 2 were excavated (i.e., extracted) directly from the outcrop. Minimal prying of outcrop blocks was needed because the fracture density was sufficiently high. Staff attempted to collect all particle sizes from Plot 2 for subsequent laboratory experiments (see Section 3), including fine-grained particles, although the fine material was not used in size distribution analysis. It was not possible to quantify the amount of fine-grained material that may have been transported into the outcrop or lost to erosion; this represents a limitation to the data collected at Plot 2, but is not expected to significantly affect results. The percentage volume of fines in a rubble pile may influence the bulking factor (Peele, 1961).

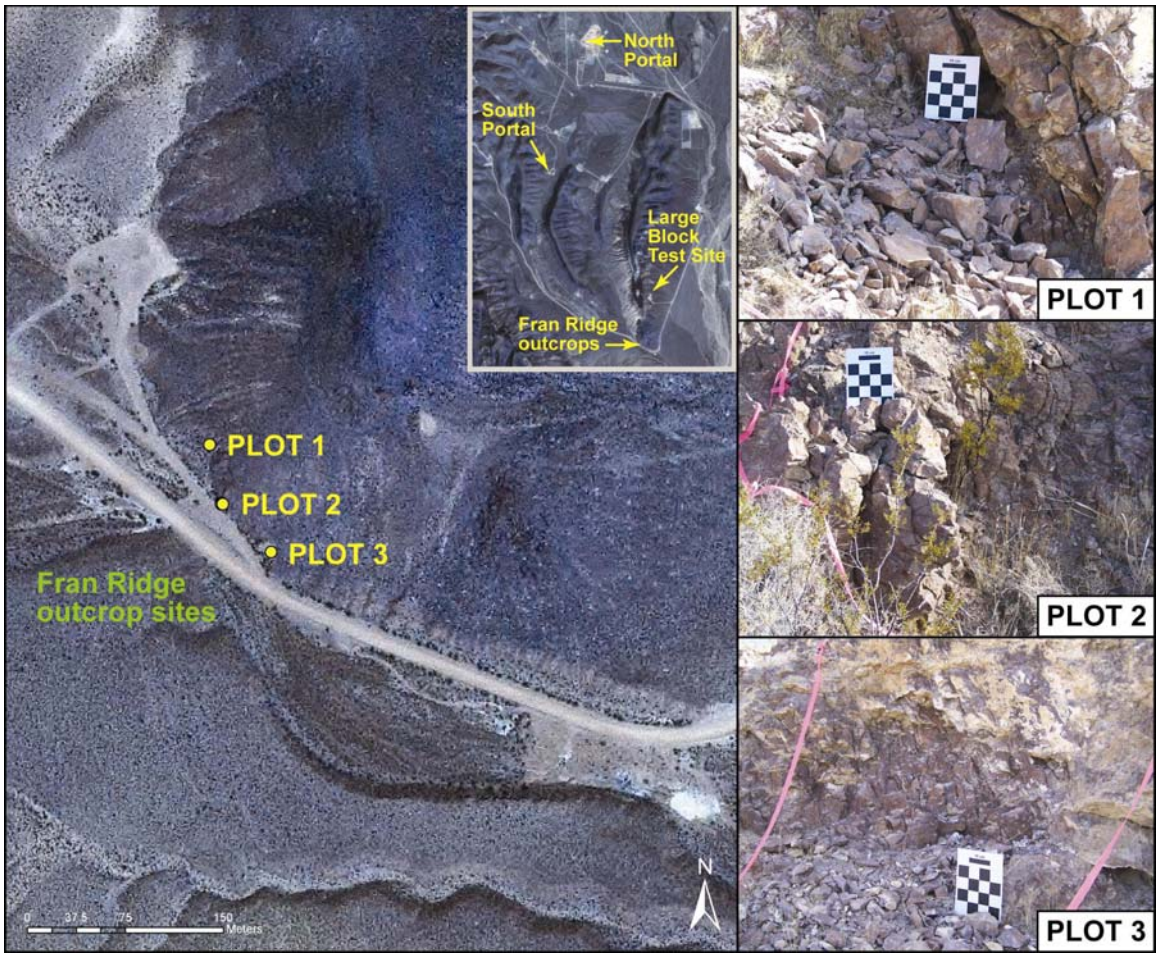

Figure 2-1. A Location Map of Fran Ridge Outcrop Sites Inset Shows Location With Respect to the Exploratory Studies Facility (ESF) at Yucca Mountain

Rubble data were recorded in the field with the following methodology: (i) clasts were photographed on a 2 by 2-cm [0.79 by 0.79-in] grid, (ii) the longest orthogonal dimensions (length, width, height) were measured, and (iii) all measurements were rounded to the nearest 0.5-cm [0.20-in] increment. Size limitations on the collection include truncations at the smallest and largest scale. The largest rock clasts collected were limited to the outcrop scale. The smallest clasts {~3–10 cm [1.18–3.94 in] in longest dimension} were too small to practically measure in the field. These clasts were binned by average size, laid out on the grid as close together as possible (representing the total length and width), and photographed as a group, with the largest and average heights recorded. Rubble particle volumes were averaged for these groups by calculating the overall length, width, and height of the collection and dividing by the number of clasts in the group.

Approximately 1,500 rubble clasts were photographed and measured during the field examination. Four 0.24-m^3 [55-gal] drums of rubble were collected for further analyses (Figure 2-2). Each drum contained a single rubble characterization site (e.g., sample drum #1 contains rubble collected and characterized from Plot 1). For Plot 2, only subareas A and B were collected. The largest clasts measured were wrapped separately on a pallet and tagged for sample identification.

Figure 2-2. Example Rubble Pile Collected From Plot 2 Outcrop at Fran Ridge

Field observations indicated that the talus primarily resulted from degradation along existing outcrop fractures. Observations included a positive correlation between higher fracture intensity and smaller clast sizes. Also, fracture set orientations contributed to the shape of rock fragments (e.g., bladed or elongate). Field observations indicated most rock clasts were bladed, elongate, or platy in shape (Figure 2-3). The least frequently encountered shape was cubic (i.e., equidimensional).

2.2 Fracture Characterization

Three primary fracture sets were defined from the Fran Ridge outcrop data (Table 2-1). Fracture data were analyzed with RockWare StereoStat® Version 1.4 (RockWare, Inc., 2004) for orientation and dispersion values to determine fracture sets. Set 1 is a north-northwest striking, steeply dipping set with an average strike and dip of 166°/73°. Mean spacing for Set 1 fractures is 7 cm [2.76 in]. Set 2 is an east-west-striking, moderately dipping set with an average strike and dip of 101°/69°. Mean spacing for Set 2 fractures is 16 cm [6.30 in]. Set 3 is a subhorizontal fracture set with a mean strike and dip of 355°/15° and spacing of 9 cm [3.54 in].

A comparison of the Fran Ridge outcrop fractures (outcrop scale) in the Tptpll to the fracture data Smart, et al. (2006) analyzed for the same zone recorded in the Detailed Line Survey in the Exploratory Studies Facility (ESF)[1] and enhanced characterization of repository block (ECRB)[2]

[1]Exploratory Studies Facility is used frequently throughout this chapter; therefore, the acronym ESF will be used.
[2]Enhanced characterization of repository block is used frequently throughout this chapter; therefore, the acronym ECRB will be used.

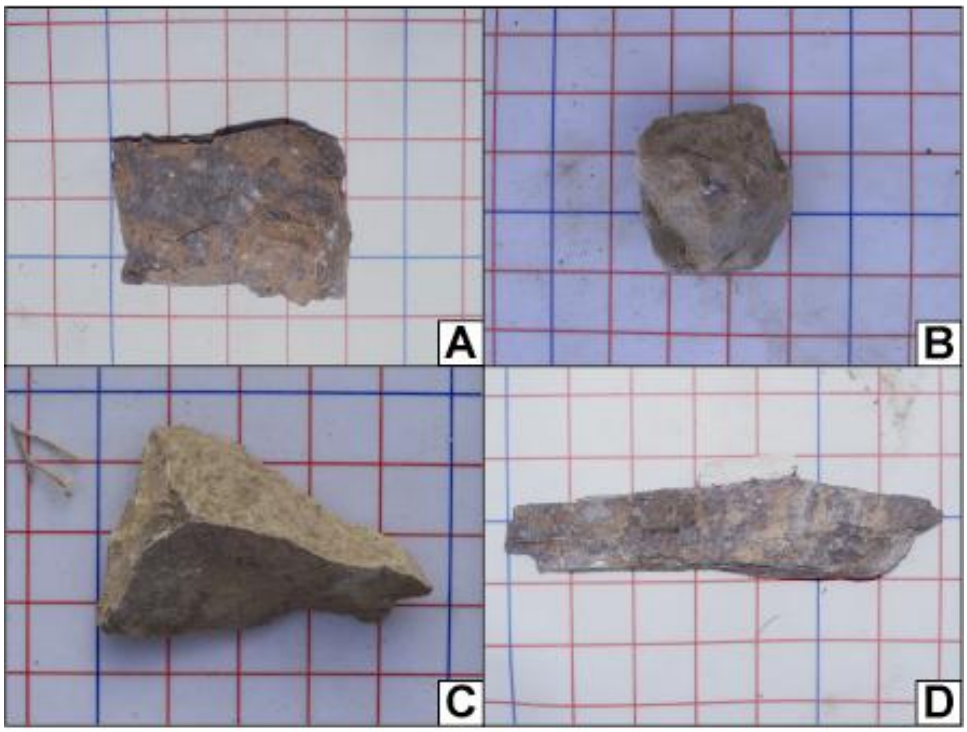

Figure 2-3. Examples of Basic Rubble Shapes. (A) Platy, (B) Cubic, (C) Bladed, and (D) Elongate. Note That Background Grid Has 2 by 2-cm [0.79 by 0.79-in] Spacing.

Table 2-1. Summary of Fran Ridge Fracture Data Collected at All Plots

Fracture Set	Mean Orientation	Angular Standard Deviation	Fisher Dispersion Coefficient*	True Spacing (cm) [in]	
				Mean	Median
Fran Ridge (this report)					
Set 1	129°/72°	64°	13.3	7.3 [2.87]	6.2 [2.44]
Set 2	101°/69°	17°	21.8	16.3 [6.42]	12.5 [4.92]
Set 3	355°/15°	12°	42.4	9.1 [3.58]	8.5 [3.35]
Table 3-7†					
Set 1	134°/82°	45°	3.3	10.8 [4.25]	3 [1.18]
Set 2	079°/82°	21°	14.6	24 [9.45]	12 [4.72]
Set 3	313°/04°	12°	47.4	10 [3.94]	6 [2.36]

*The Fisher dispersion coefficient (also referred to as the concentration parameter) is a measure of the degree to which spherical data are concentrated around the mean (Fisher, N.I., T. Lewis, and B.J.J. Embleton. *Statistical Analysis of Spherical Data.* Cambridge, United Kingdom: Cambridge University Press. 1993). Larger values of the Fisher dispersion coefficient indicate tighter clustering (i.e., less dispersion).
†Smart, K.J., D.Y. Wyrick, P.S. Landis, and D.J. Waiting. "Summary and Analysis of Subsurface Fracture Data From the Topopah Spring Tuff Upper Lithophysal, Middle Nonlithophysal, Lower Lithophysal, and Lower Nonlithophysal Zones at Yucca Mountain, Nevada." CNWRA 2005-04. ML060660009. San Antonio, Texas: Center for Nuclear Waste Regulatory Analyses. 2006.

(drift scale) shows similar fracture orientations (strike and dip) and spacing between these two sites (Figures 2-4 and 2-5). Both the outcrop-scale and drift-scale fracture analyses indicate three primary fracture sets: (i) a north-northeast striking, steeply dipping set; (ii) an east-west-striking, steeply dipping set; and (iii) a subhorizontal set. The mean orientation of these three primary sets measured at Fran Ridge fall within the angular standard deviation (representing the degree of scatter) of the mean fracture set data observed in the ESF and ECRB. Fracture lengths between the two sites are not directly comparable (outcrop scale versus drift scale) as most fracture tracelengths at the outcrop were truncated because of the small exposures. A comparison of fracture spacing at the outcrop scale to the small-scale fracture data collected in the ECRB cross drift (cf., Table 2-1 this report; Smart, et al., 2006, Table 3-7) shows similar values for fracture spacing.

Some variations in fracture orientations and spacing are observed for each plot (Tables 2-2 to 2-4). Notably, Plot 3 differs from Plots 1 and 2 (and the ESF/ECRB fracture data) both in fracture set orientations and in fracture spacing. Fracture Set 2 (east-west striking, moderately dipping) was not found at Plot 3; instead, north-northwest-striking, steeply dipping and north-northeast-striking, steeply dipping fracture sets were observed. Plot 3 had smaller fracture spacing values overall. This variation in Plot 3 fracture data is likely due to its proximity to a mapped normal fault near the southeast end of Fran Ridge (Day, et al., 1998).

2.3 Rubble Characterization

2.3.1 Clast Shape Distribution

The literature reviewed shows that rubble clast shape influences bulking factor (Pappas and Mark, 1993). To characterize the shapes distribution of rubble, a classification system that captures the wide range of clast shape is required. A literature search of the types of clast shape classifications systems indicates that a modified Sneed and Folk (1958) organization that includes shape ranges from cubic (equidimensional), platy (tabular), bladed, and elongate (rod) is suitable for these analyses (Sneed and Folk, 1958; Graham and Midgley, 2000). Sneed and Folk (1958) diagrams, employing ratios of the three orthogonal particle axes, have been advocated as the most appropriate method for unbiased presentation of primary particle shape data. A Sneed and Folk (1958) diagram is scaled such that independent (although related) variables can be plotted for one axis without necessarily affecting the other two. For any given particle, the values of the three axes (length, width, and height) are independent, except that, by definition, Length≥Width≥Height. This type of triangular diagram differs from traditional ternary plots where the three variables plotted represent relative proportions of a whole (i.e., a decrease in one variable will produce increases in one or both of the other variables). The four major shape classifications (cubic, platy, elongate, and bladed) are illustrated in Figure 2-6 to show the general block shapes and their locations on the chart.

For the major classifications, subdivisions are grouped such that cubic = all cubic values; platy = cubic-platy + platy + very platy; bladed = cubic-bladed + bladed + very bladed; and elongate = cubic-elongate + elongate + very elongate (Figure 2-6). The major shape classifications could be grouped slightly differently (e.g., cubic could include cubic + cubic platy + cubic elongate + cubic bladed). Both values are provided in this report. The most common rubble shape was bladed fragments, representing 39–48 percent of all rubble clasts; elongate shapes represented 26-31 percent of all rubble. These two primary shapes combined comprised 65–79 percent of the outcrop rubble measured. Clast shape data for all the Fran Ridge outcrop samples are illustrated in Figures 2-7 to 2-10.

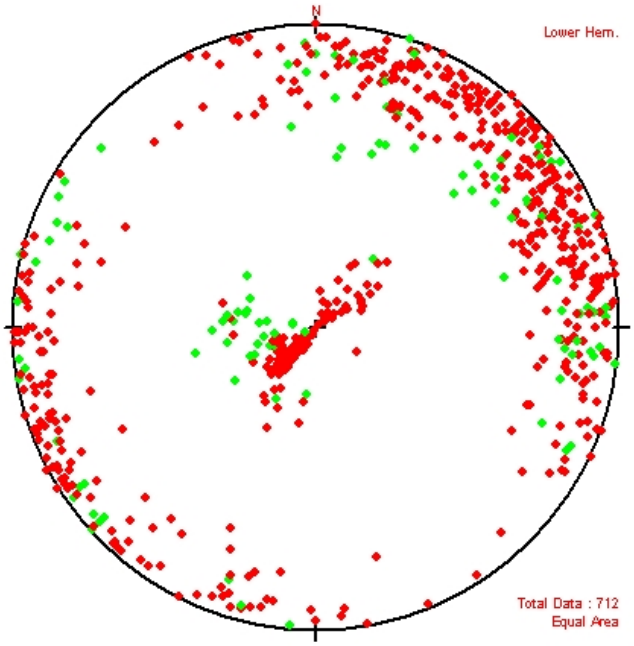

Figure 2-4. Equal-Area Stereonet Plot of Poles to Fracture Planes From Fracture Orientation Data Collected at Fran Ridge Outcrop (Green) and the ESF/ECRB Detailed Line Survey Small-Scale Fracture Data (Red). (Smart, et al., 2006, Figure 3-10)

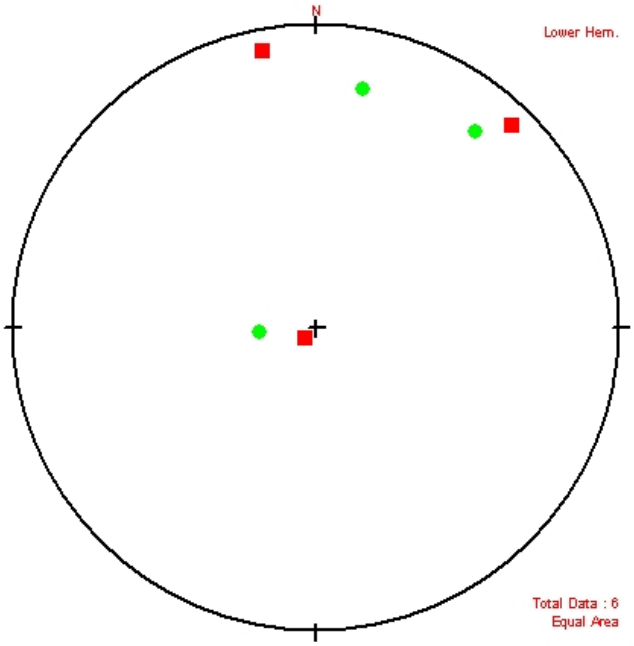

Figure 2-5. Equal-Area Stereonet Plot of Poles to the Mean Fracture Set Planes From Table 2-1 (Green Circles From Fran Ridge, Red Squares From ESF/ECRB)

Table 2-2. Summary of Fran Ridge Fracture Data Collected at Plot 1		
Fracture Set	**Mean Orientation**	**True Spacing (cm) [in] Mean**
Set 1	170°/71°	10.2 [4.02]
Set 2	097°/24°	12.1 [4.76]
Set 3	007°/24°	15.4 [6.06]

Table 2-3. Summary of Fran Ridge Fracture Data Collected at Plot 2		
Fracture Set	**Mean Orientation**	**True Spacing (cm) [in] Mean**
Set 1	164°/73°	7.6 [2.99]
Set 2	102°/69°	17.2 [6.77]
Set 3	349°/17°	8.4 [3.31]

Table 2-4. Summary of Fran Ridge Fracture Data Collected at Plot 3		
Fracture Set	**Mean Orientation**	**True Spacing (cm) [in] Mean**
Set 1	172°/76°	4.3 [1.69]
Set 2	—	—
Set 3	353°/13°	6.8 [2.68]
Set 4	332°/85°	3.64 [1.43]
Set 5	022°/83°	2.75 [1.08]

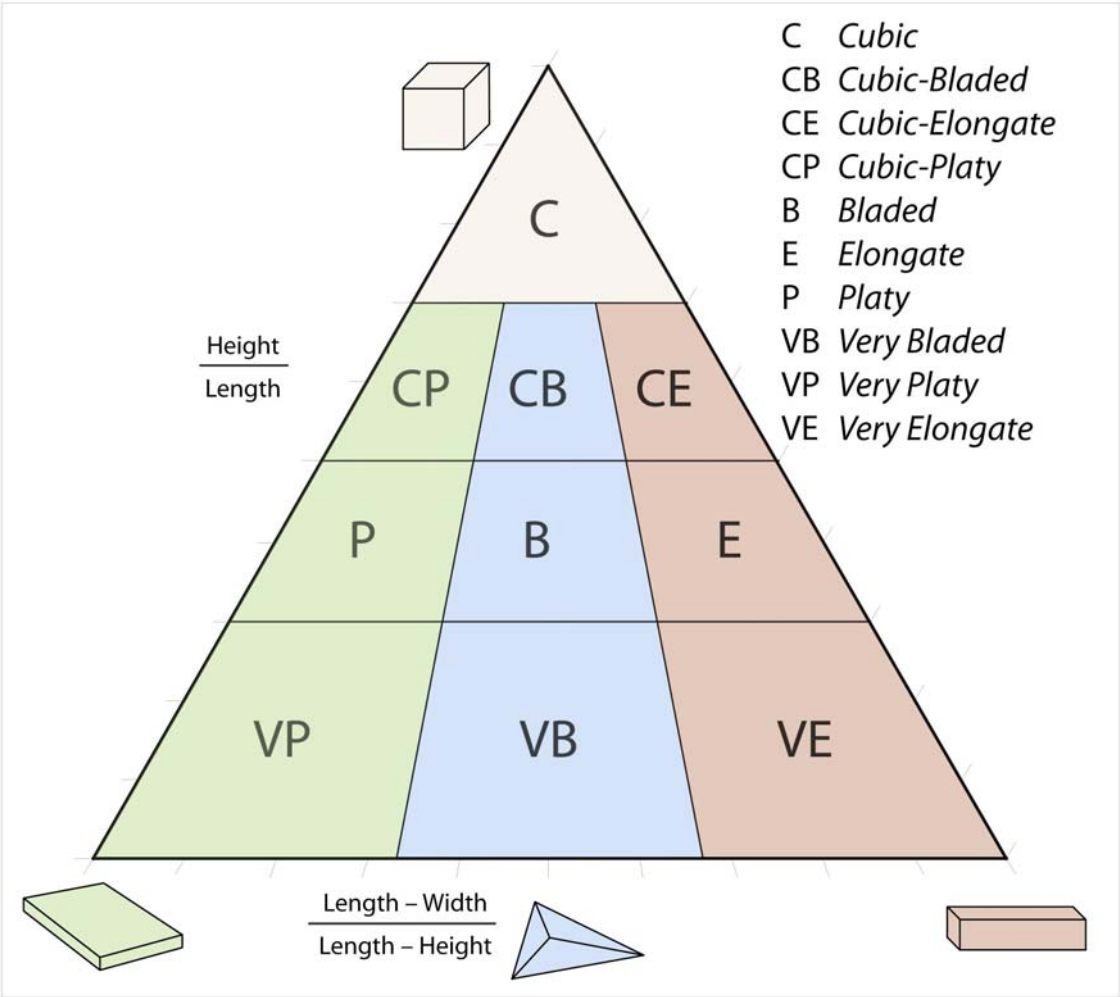

Figure 2-6. A Modified Sneed and Folk Diagram Representation of Particle Shape (Sneed and Folk, 1958; Graham and Midgley, 2000). Sneed and Folk Diagrams Employ Ratios of the Three Orthogonal Particle Axes To Present Primary Particle Shape Data.

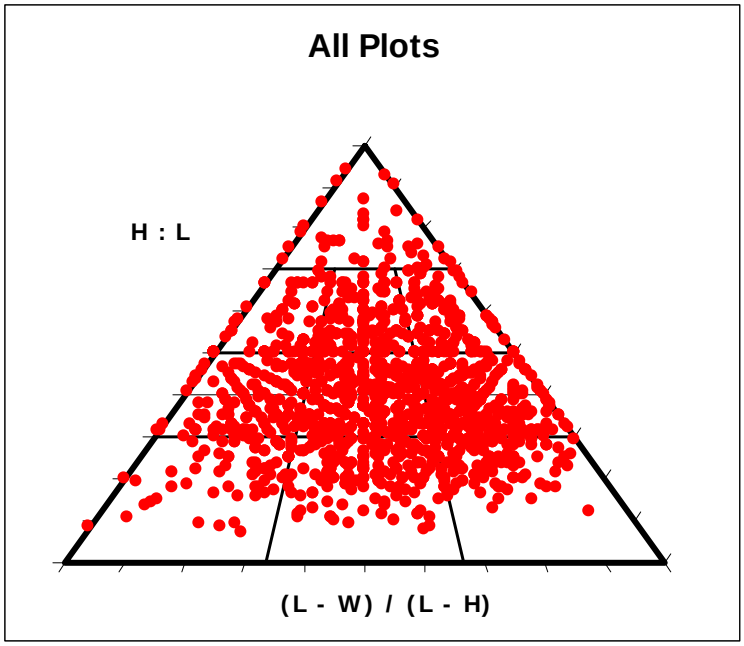

Figure 2-7. Modified Sneed and Folk Diagram of All Rubble Shape Data

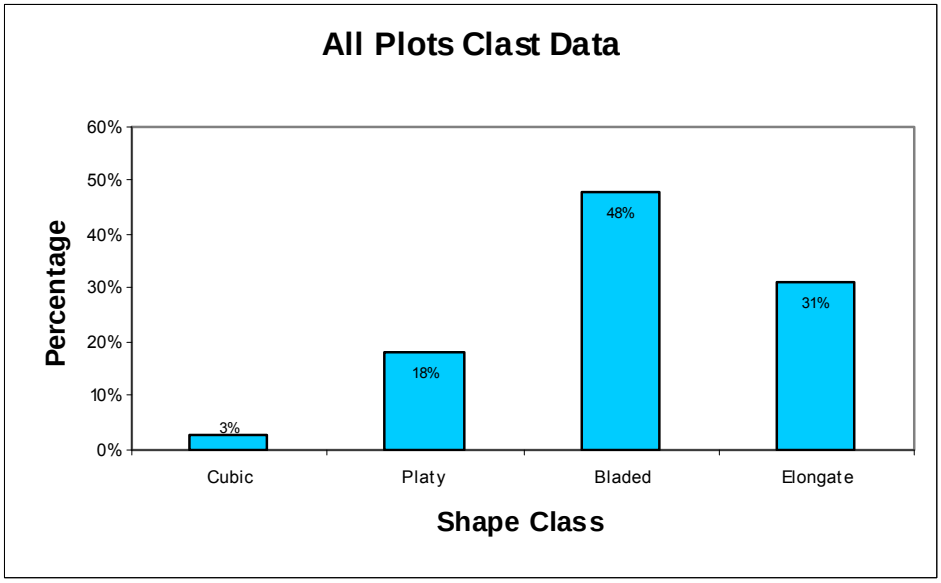

Figure 2-8. Rubble Shape Major Classification by Percentage for All Rubble Shape Data. In This Chart, Cubic = Cubic; Platy = Cubic-Platy + Platy + Very Platy; Bladed = Cubic-Bladed + Bladed + Very Bladed; Elongate = Cubic-Elongate + Elongate + Very Elongate.

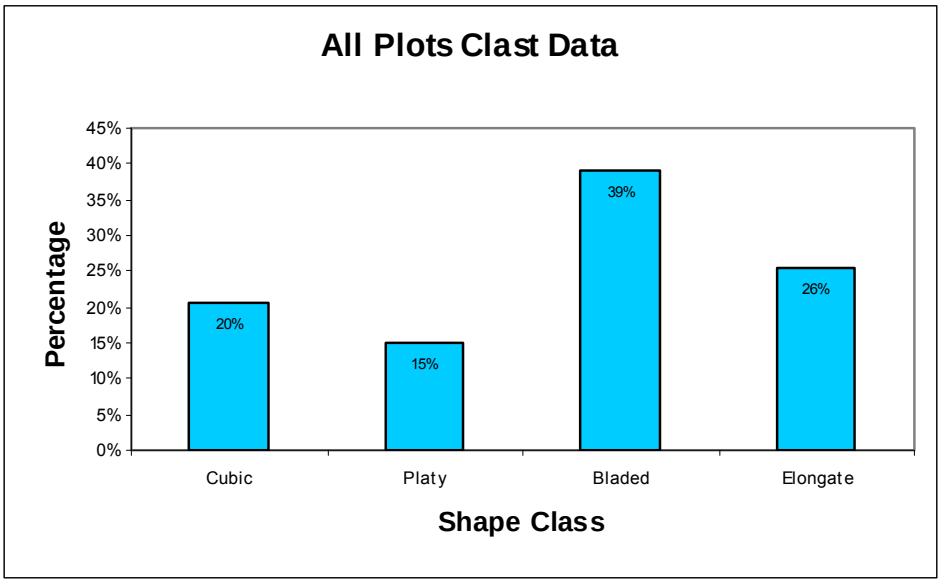

Figure 2-9. Rubble Shape Major Classification by Percentage for All Rubble Shape Data. In This Chart, Cubic = Cubic + Cubic Platy + Cubic Elongate + Cubic Bladed; Platy = Platy + Very Platy; Bladed = Bladed + Very Bladed; Elongate = Elongate + Very Elongate.

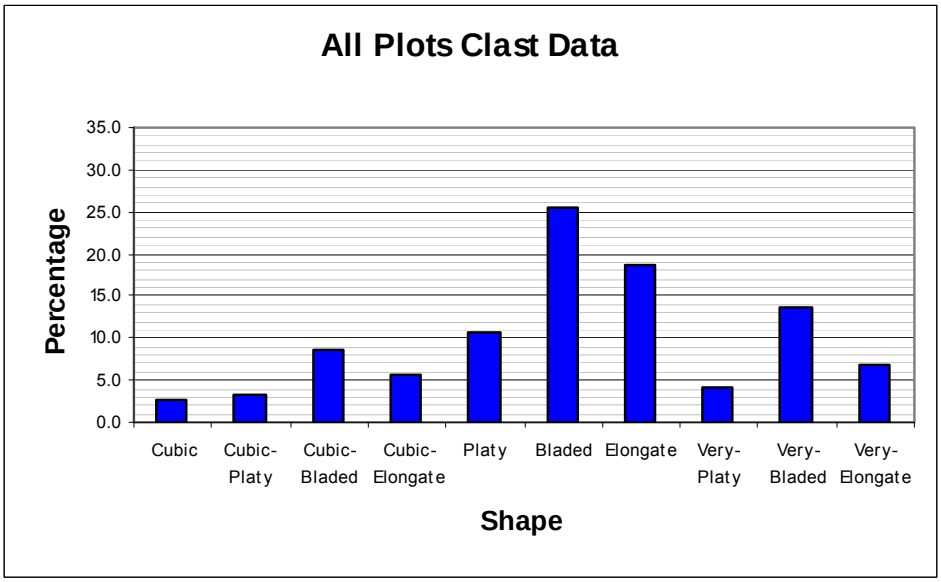

Figure 2-10. Rubble Shape Classification Detail by Percentage for All Rubble Shape Data

Plot 1A

Plot 1A rubble was collected from the talus pile located directly beneath the outcrop (Figure 2-11). Rubble fragments from this location are primarily bladed and elongate in shape (Figures 2-12 to 2-15).

Figure 2-11. Field Photograph of Talus Pile Location for Plot 1A

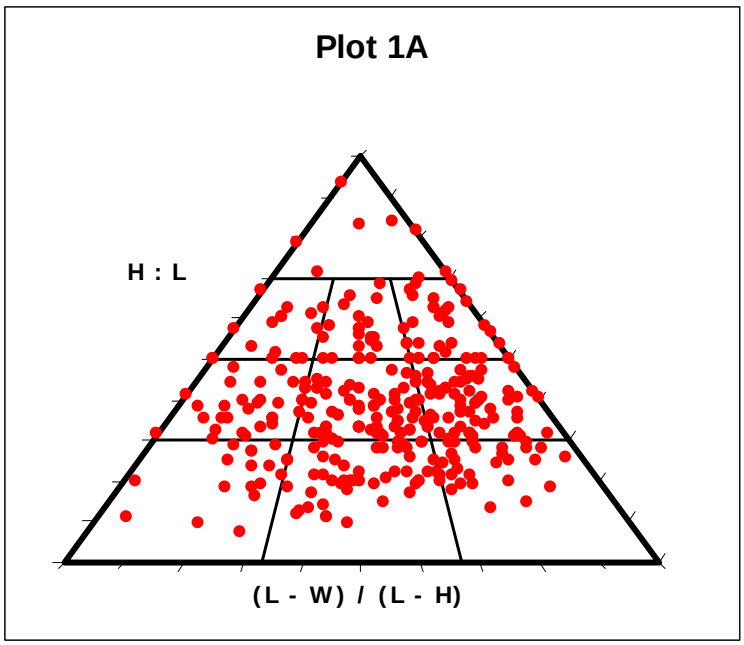

Figure 2-12. Modified Sneed and Folk Diagram of Plot 1A Rubble Shape Data

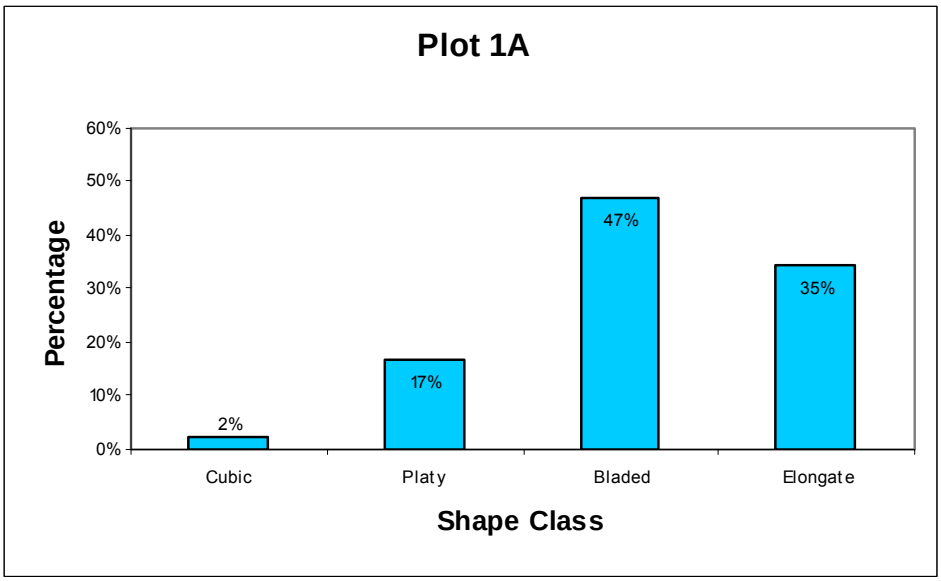

Figure 2-13. Rubble Shape Major Classification by Percentage for Plot 1A Rubble Shape Data. In This Chart, Cubic = Cubic; Platy = Cubic-Platy + Platy + Very Platy; Bladed = Cubic-Bladed + Bladed + Very Bladed; Elongate = Cubic-Elongate + Elongate + Very Elongate.

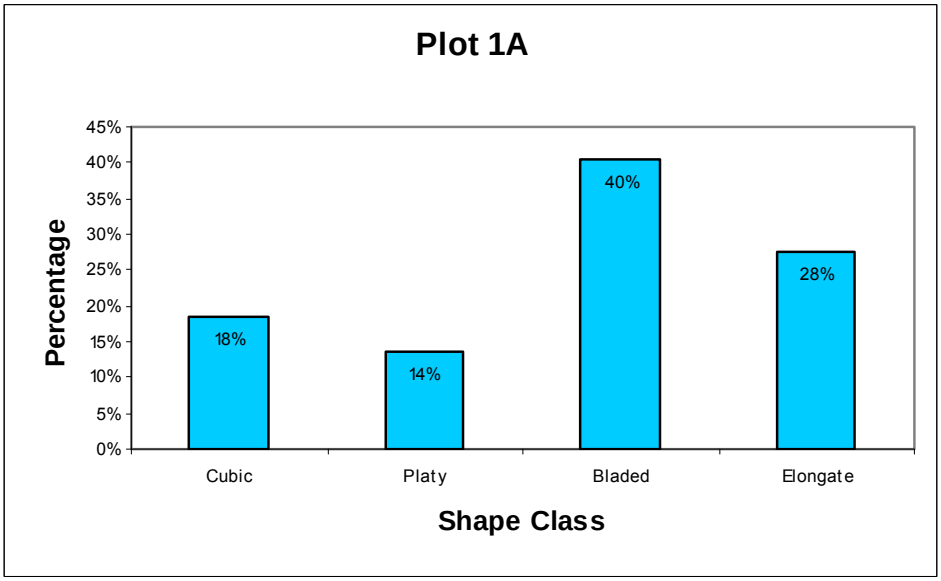

Figure 2-14. Rubble Shape Major Classification by Percentage for Plot 1A Rubble Shape Data. In This Chart, Cubic = Cubic + Cubic Platy + Cubic Elongate + Cubic Bladed; Platy = Platy + Very Platy; Bladed = Bladed + Very Bladed; Elongate = Elongate + Very Elongate.

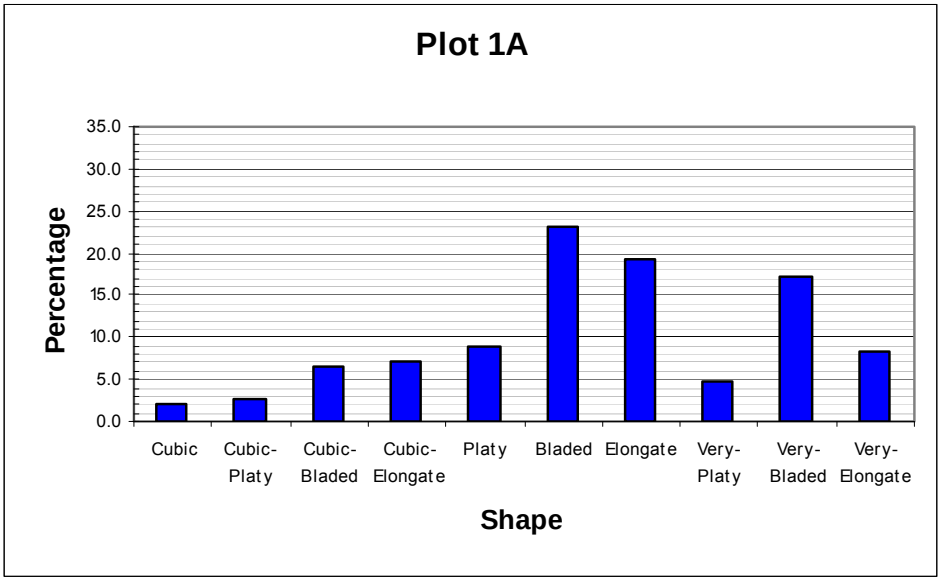

Figure 2-15. Rubble Shape Classification Detail by Percentage for Plot 1A Rubble Shape Data

Plot 2A

Plot 2A rubble was extracted directly from the outcrop with minimal force to provide the most "pristine" rubble collection possible (Figure 2-16). Rubble fragments from this location are primarily bladed and elongate in shape (Figures 2-17 to 2-20).

Figure 2-16. Field Photograph of Rubble Collection Area Plot 2

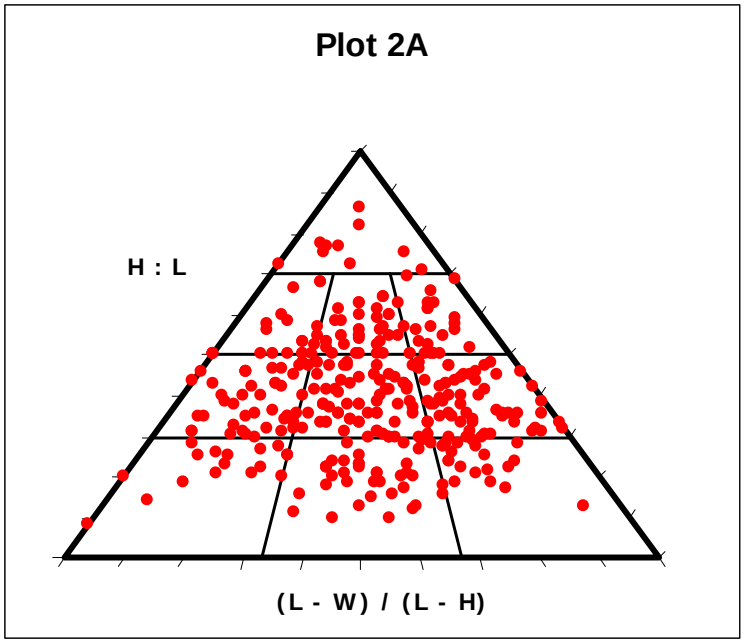

Figure 2-17. Modified Sneed and Folk Diagram of Plot 2A Rubble Shape Data

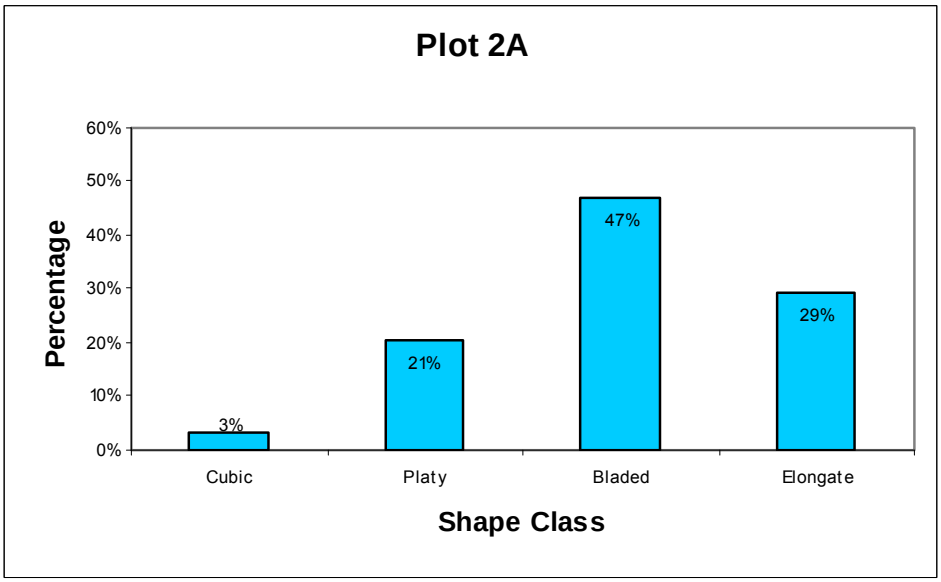

Figure 2-18. Rubble Shape Major Classification by Percentage for Plot 2A Rubble Shape Data. In This Chart, Cubic = Cubic; Platy = Cubic-Platy + Platy + Very Platy; Bladed = Cubic-Bladed + Bladed + Very Bladed; Elongate = Cubic-Elongate + Elongate + Very Elongate.

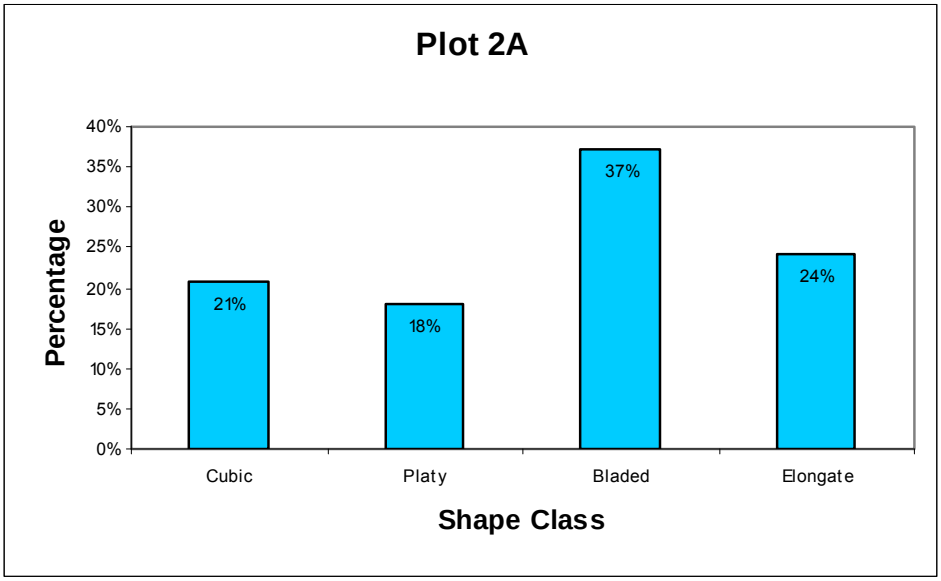

Figure 2-19. Rubble Shape Major Classification by Percentage for Plot 2A Rubble Shape Data. In This Chart, Cubic = Cubic + Cubic Platy + Cubic Elongate + Cubic Bladed; Platy = Platy + Very Platy; Bladed = Bladed + Very Bladed; Elongate = Elongate + Very Elongate.

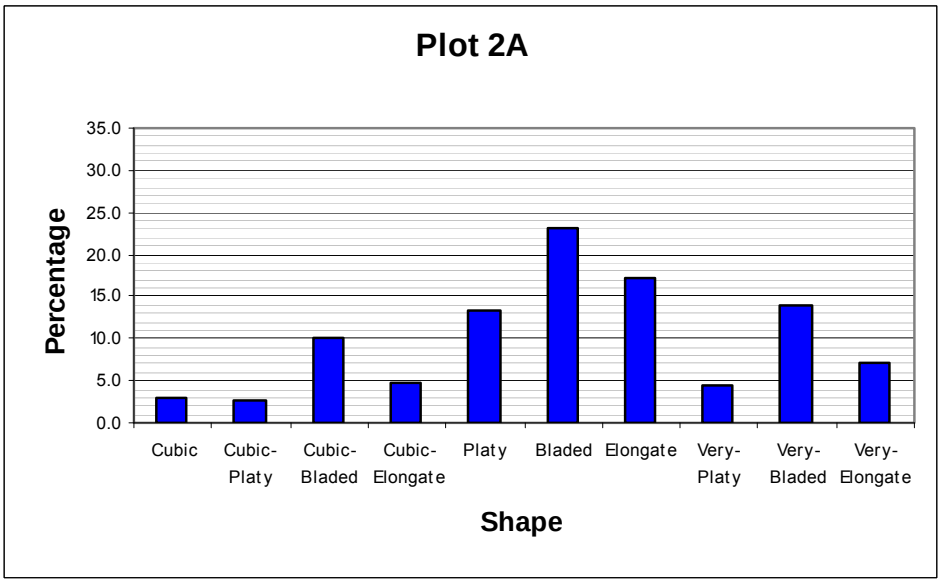

Figure 2-20. Rubble Shape Classification Detail by Percentage for Plot 2A Rubble Shape Data

Plot 2B

Plot 2B rubble was extracted directly from the outcrop with minimal force to provide the most "pristine" rubble collection possible. Plot 2B was located directly above Plot 2A. Rubble fragments from this location are primarily bladed and elongate in shape (Figures 2-21 to 2-24).

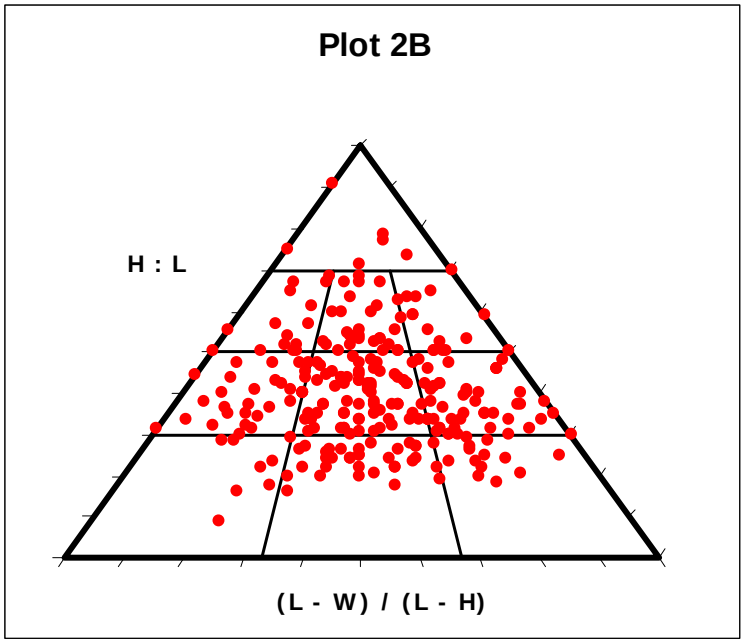

Figure 2-21. Modified Sneed and Folk Diagram of Plot 2B Rubble Shape Data

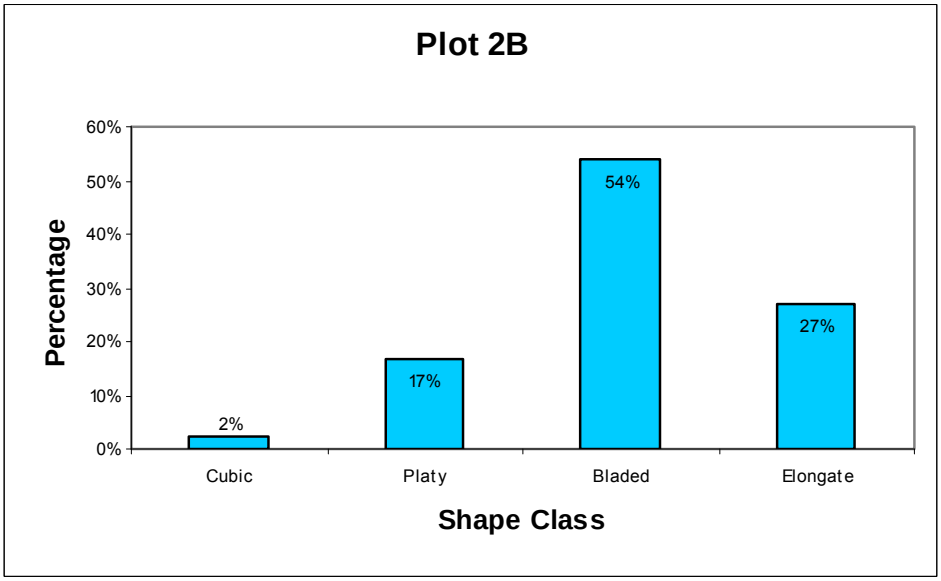

Figure 2-22. Rubble Shape Major Classification by Percentage for Plot 2B Rubble Shape Data. In This Chart, Cubic = Cubic; Platy = Cubic-Platy + Platy + Very Platy; Bladed = Cubic-Bladed + Bladed + Very Bladed; Elongate = Cubic-Elongate + Elongate + Very Elongate.

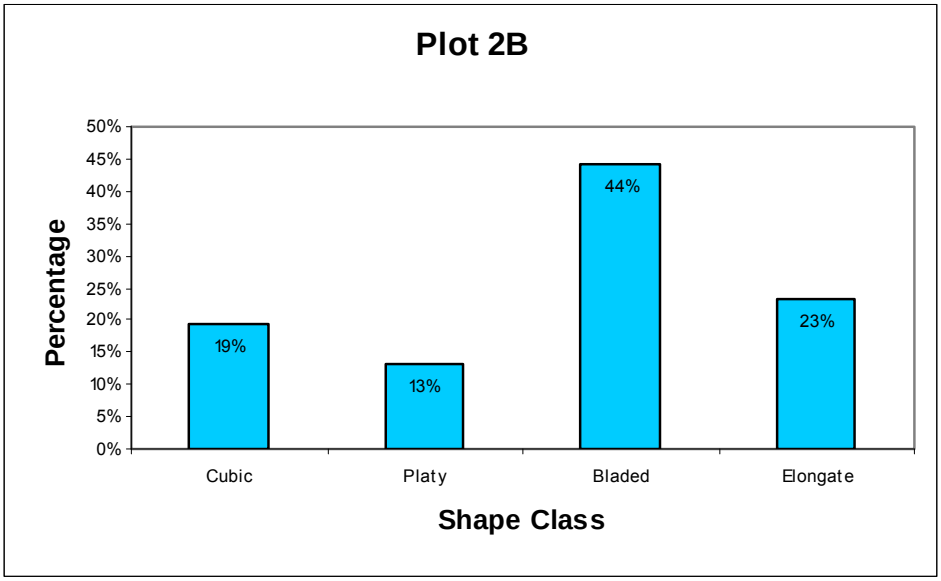

Figure 2-23. Rubble Shape Major Classification by Percentage for Plot 2B Rubble Shape Data. In This Chart, Cubic = Cubic + Cubic Platy + Cubic Elongate + Cubic Bladed; Platy = Platy + Very Platy; Bladed = Bladed + Very Bladed; Elongate = Elongate + Very Elongate.

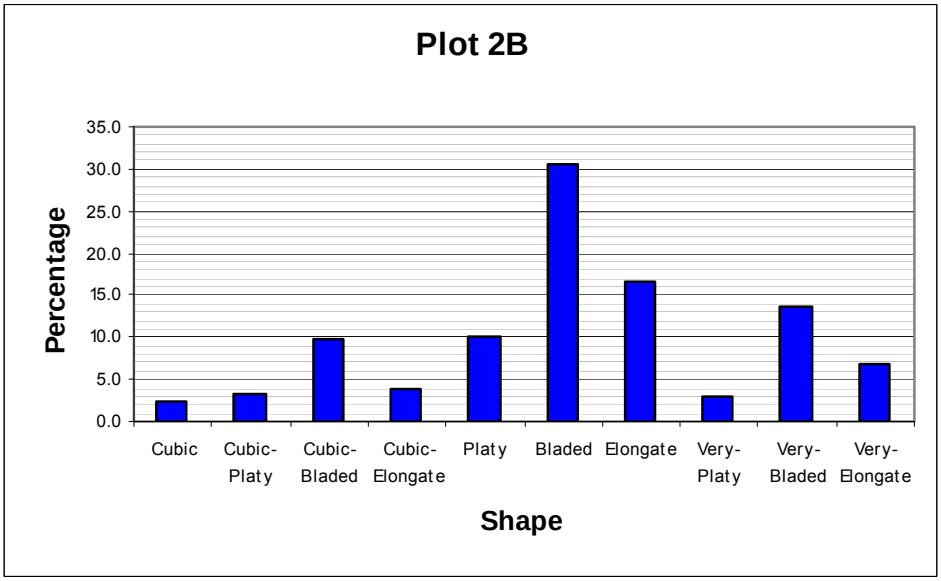

Figure 2-24. Rubble Shape Classification Detail by Percentage for Plot 2B Rubble Shape Data

Plot 2C

Plot 2C rubble was extracted directly from the outcrop with minimal force to provide the most "pristine" rubble collection possible. Plot 2C was located directly to the right (east) of Plot 2A. The rubble fragments from this subarea were measured in the field, but not collected as samples due to space limitations. Rubble fragments from this location are primarily bladed and elongate in shape (Figures 2-25 to 2-28).

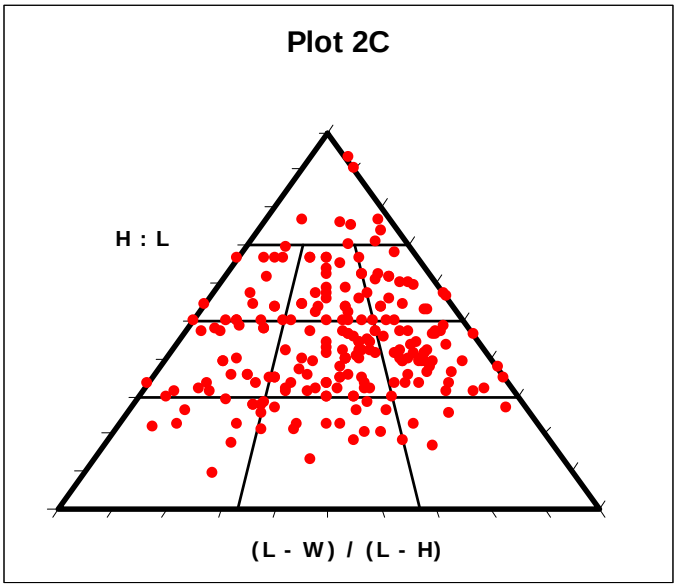

Figure 2-25. Modified Sneed and Folk Diagram of Plot 2C Rubble Shape Data

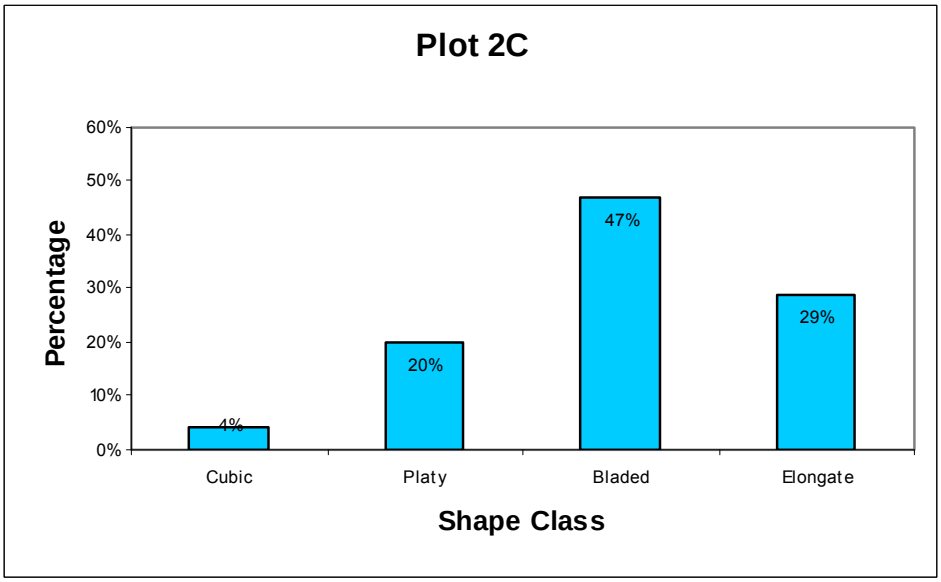

Figure 2-26. Rubble Shape Major Classification by Percentage for Plot 2C Rubble Shape Data. In This Chart, Cubic = Cubic; Platy = Cubic-Platy + Platy + Very Platy; Bladed = Cubic-Bladed + Bladed + Very Bladed; Elongate = Cubic-Elongate + Elongate + Very Elongate.

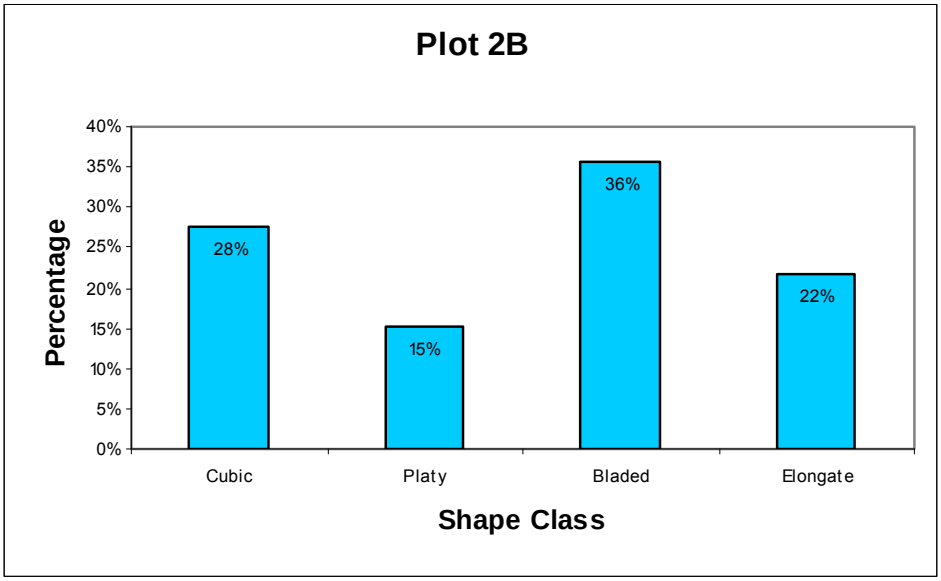

Figure 2-27. Rubble Shape Major Classification by Percentage for Plot 2C Rubble Shape Data. In This Chart, Cubic = Cubic + Cubic Platy + Cubic Elongate + Cubic Bladed; Platy = Platy + Very Platy; Bladed = Bladed + Very Bladed; Elongate = Elongate + Very Elongate.

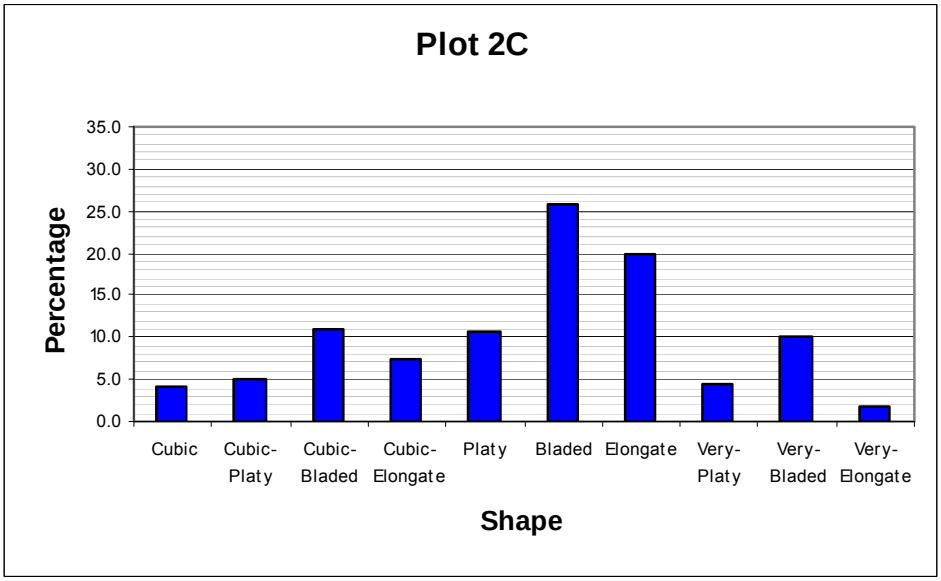

Figure 2-28. Rubble Shape Classification Detail by Percentage for Plot 2C Rubble Shape Data

Plot 3

Plot 3 rubble was collected from the talus pile located directly beneath the outcrop (Figure 2-29). Rubble fragments from this location are primarily bladed and elongate in shape (Figures 2-30 to 2-33).

Figure 2-29. Field Photograph of Talus Pile Location for Plot 3. Note That Higher Fracture Frequency at This Location Correlated With Smaller Rubble Clast Size.

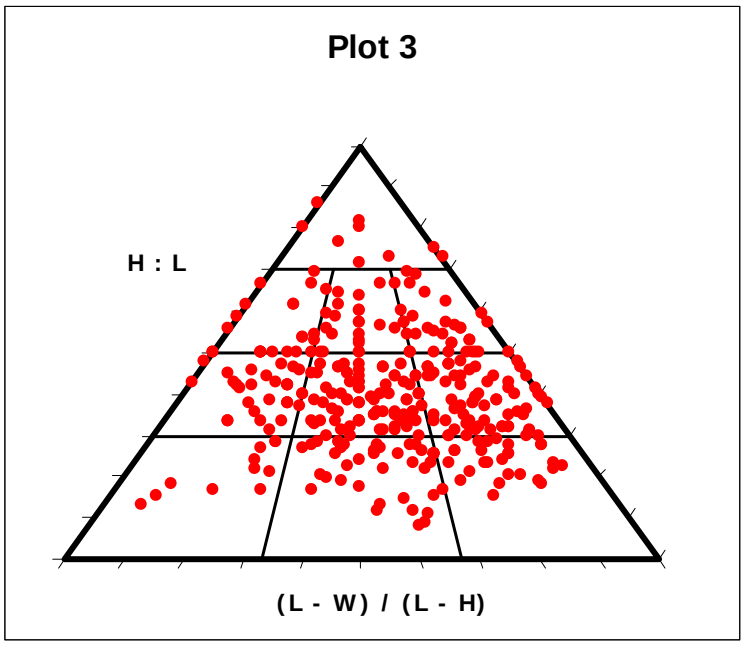

Figure 2-30. Modified Sneed and Folk Diagram of Plot 3 Rubble Shape Data

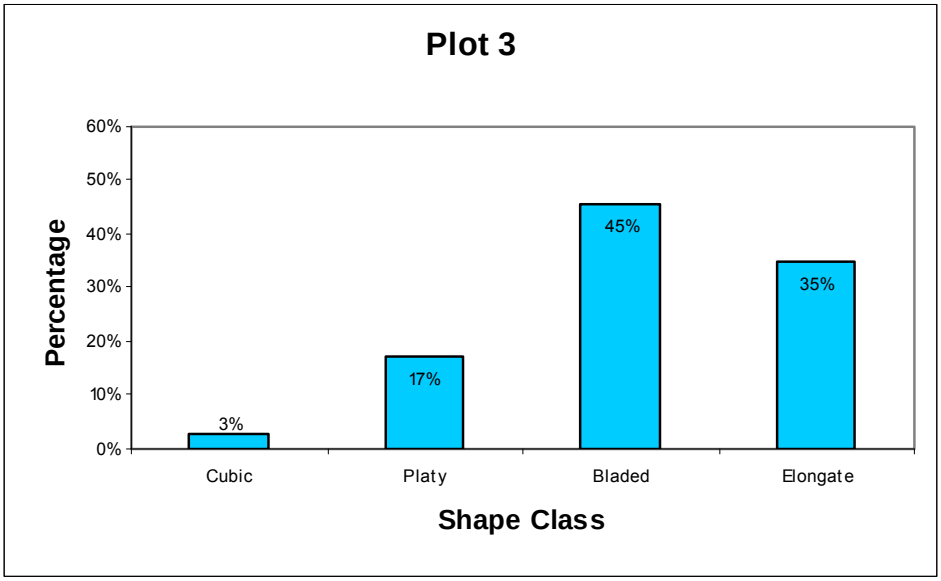

Figure 2-31. Rubble Shape Major Classification by Percentage for Plot 3 Rubble Shape Data. In This Chart, Cubic = Cubic; Platy = Cubic-Platy + Platy + Very Platy; Bladed = Cubic-Bladed + Bladed + Very Bladed; Elongate = Cubic-Elongate + Elongate + Very Elongate.

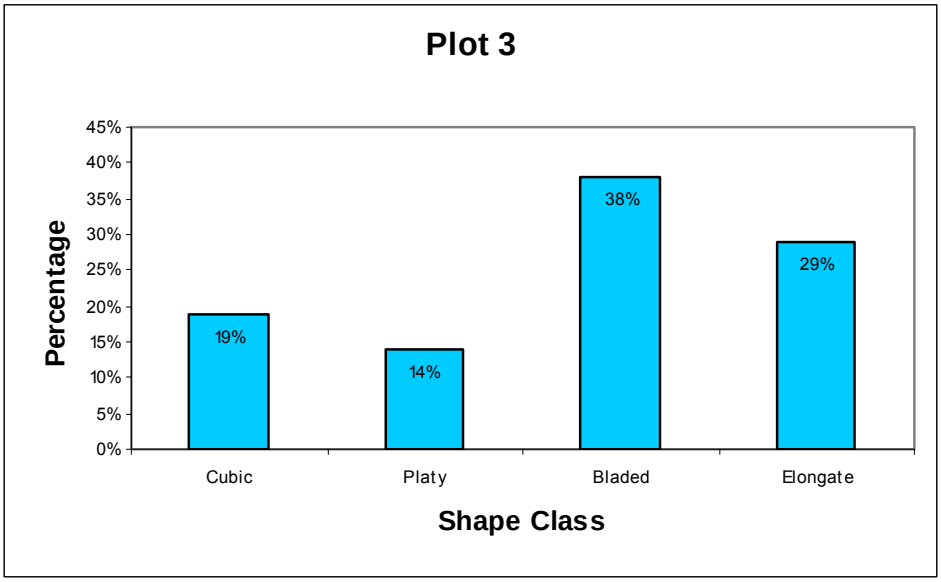

Figure 2-32. Rubble Shape Major Classification by Percentage for Plot 3 Rubble Shape Data. In This Chart, Cubic = Cubic + Cubic Platy + Cubic Elongate + Cubic Bladed; Platy = Platy + Very Platy; Bladed = Bladed + Very Bladed; Elongate = Elongate + Very Elongate.

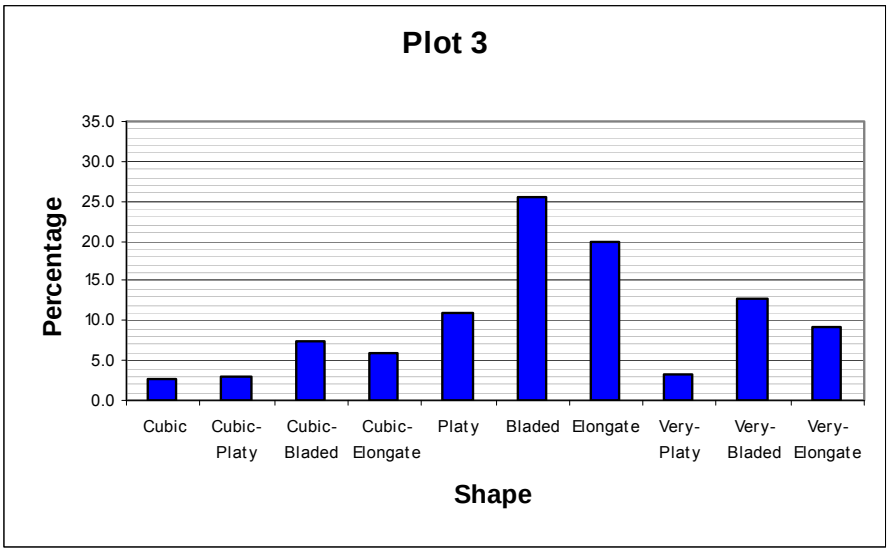

Figure 2-33. Rubble Shape Classification Detail by Percentage for Plot 3 Rubble Shape Data

2.3.2 Clast Size Distribution

Rubble clast size (length, width, and height) was measured in the field. The majority (94 percent) of clast lengths (defined as the longest orthogonal dimension) were between 5 and 20 cm [1.97 and 7.87 in] with 50 percent of the fragments measuring ≤ 11 cm [4.33 in] (Figures 2-34 and 2-35). Clast widths (Figures 2-34 and 2-35) in the intermediate orthogonal dimension primarily ranged between 3 and 15 cm [1.18 and 5.91 in] (96 percent) with half of the fragments ≤ 7.5 cm [2.95 in]. Heights (the shortest dimension; Figures 2-34 and 2-35) primarily ranged from 1 to 8 cm [0.39 to 3.15 in] (94 percent) with 50 percent ≤ 5 cm [1.97 in]. The majority (88 percent) of rubble clasts had volumes between 100 and 1,000 cm^3 [6.10 and 61.02 in^3] (Figure 2-36), with the median volume ≤ 3,300 cm^3 [201.38 in^3] (Figure 2-37).

Rubble size measurements are limited due to the data measurement methodology in the field. Specifically, the rubble measured in the field had a limited size range {0.5 cm [0.20 in] to a maximum of 65 cm [25.59 in]; Figure 2-34}. Additionally, all measurements were rounded to the nearest 0.5-cm [0.20-in] increment. This combines to produce a limited number of bins, both in absolute values {e.g., height values of 3.0 cm [1.18 in] occur most often; Figure 2-34} and in ratios (e.g., width/height ratios of 4:2, 6:3, and 10:5 are all equal to 2; Figure 2-38). There is also a (likely) human tendency to round to the nearest whole number increment, which can be seen in the data (e.g., Figure 2-34). Although size gradation curves were found to be relatively insensitive to maximum particle size (Pappas and Mark, 1993), the smallest particle sizes may be underrepresented in the rubble analyses. The size gradation curves for the Fran Ridge rubble, therefore, represent the range that was measured at the outcrop scale. Although the size distributions are generally similar, there are variations in the rubble size characteristics by plot (Figures 2-39 to 2-48). Plot 1, collected from the talus pile, has median length, width, and height values of 5, 8, and 12 cm [1.97, 3.15, and 4.72 in], respectively, with 50 percent of the rubble clast volume ≤ 2,329 cm^3 [142.12 in^3]. Plot 2A, removed *in situ*, had the largest range of particle sizes {from 0.5 to 65 cm [0.20 to 25.59 in]}; the large clasts removed from Plot 2A contribute to the median volume for this outcrop at ≤ 13,629 cm^3 [831.69 in^3]. Conversely, Plot 3 had overall smaller clast sizes {from 1 to 23 cm [0.39 to 9.06 in]}, with half of the sample ≤344 cm^3 [20.99 in^3]. This is likely due to smaller fracture spacing at Plot 3 (cf., Table 4 to Figure 2-47).

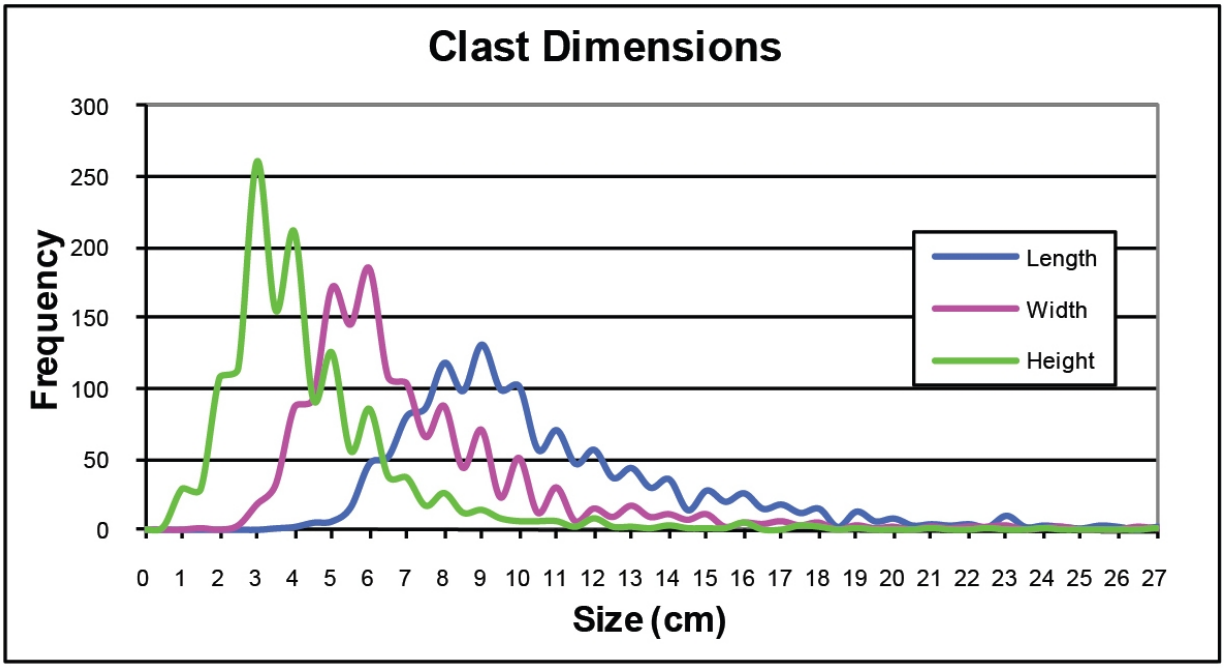

Figure 2-34. Frequency of Length (Longest Orthogonal Dimension) Measurements. All Clasts Measured Are Shown.

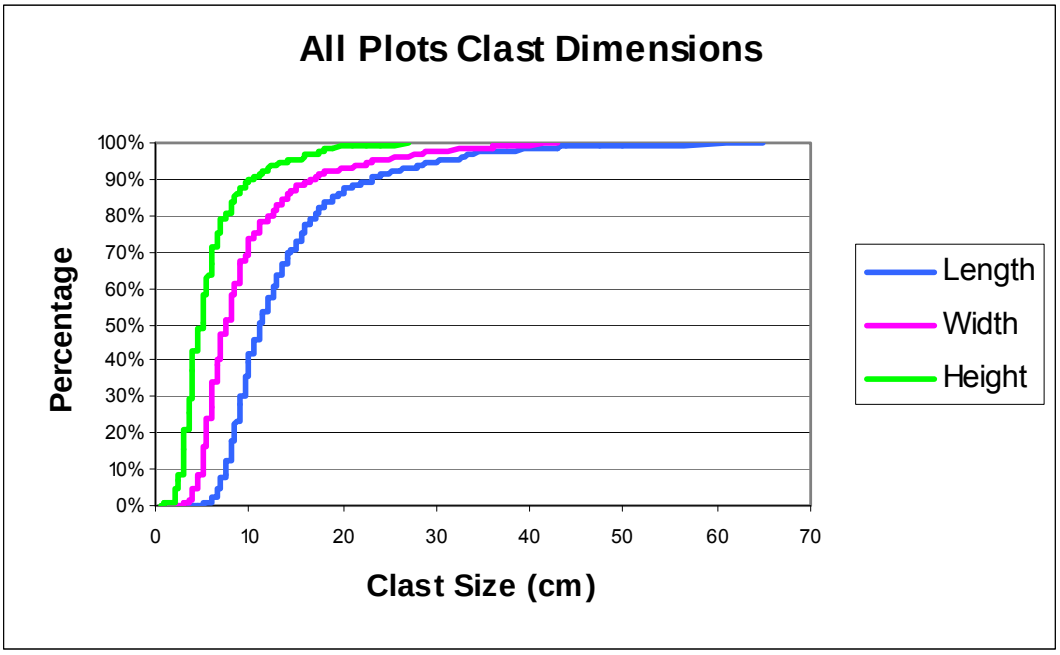

Figure 2-35. Cumulative Frequency Distribution Plot of Rubble Clast Length, Width, and Height From All Plots

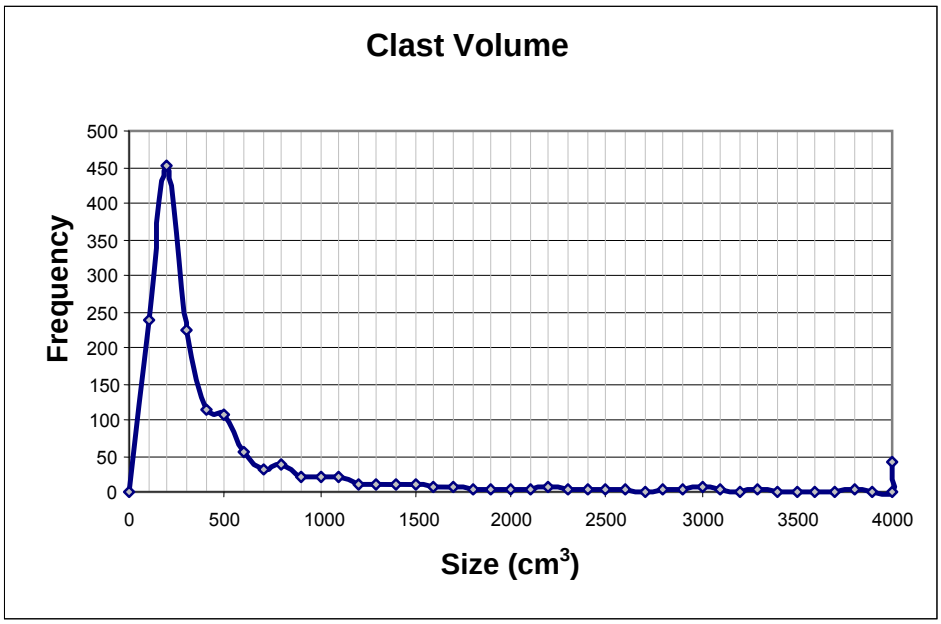

Figure 2-36. Frequency of Clast Volume. Note That Volume Measurements Are Truncated at 4,000 cm^3 [244.09 in^3] To Illustrate Smaller Values.

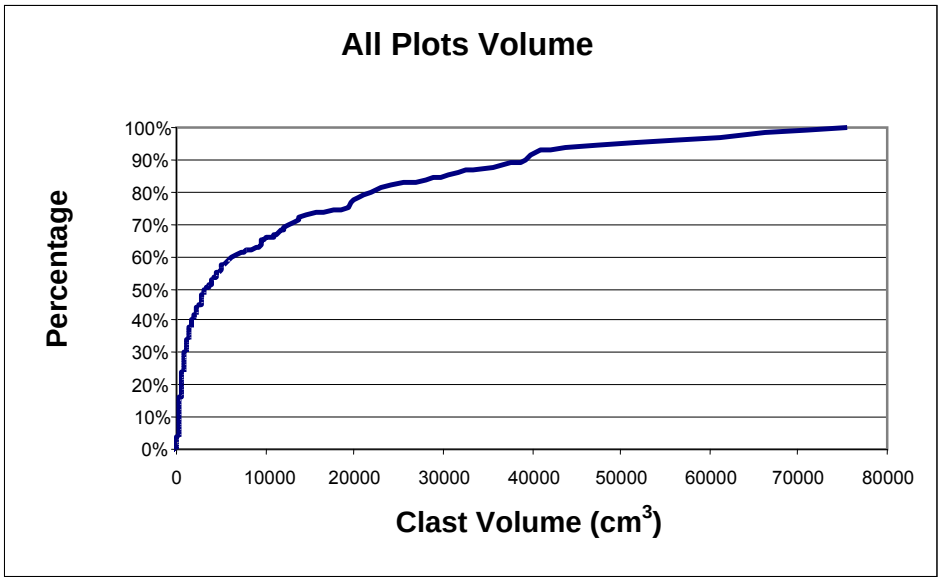

Figure 2-37. Cumulative Frequency Distribution Plot of Rubble Clast Volume From All Plots

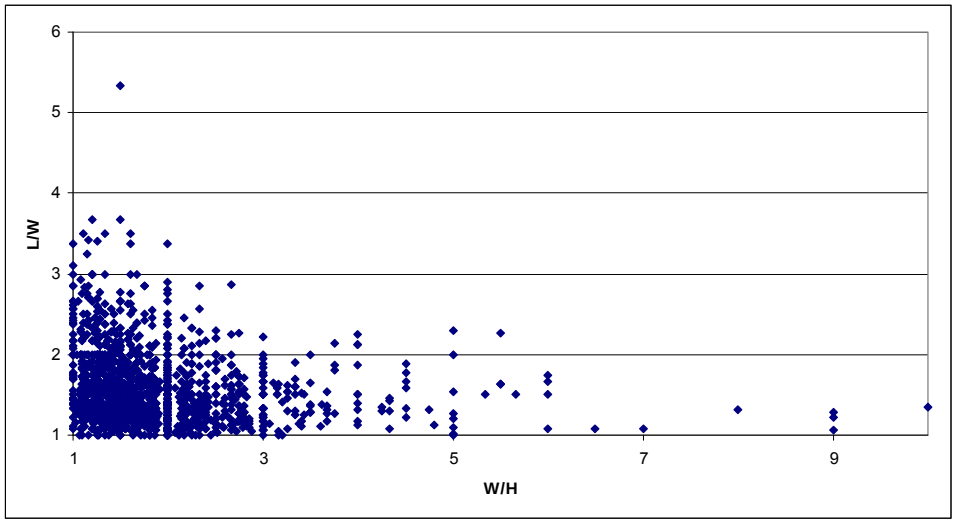

Figure 2-38. Plot of (Length/Width) Versus (Width/Height) Illustrates the Limited Binning Effect Described on Size Distributions. All Clasts Measured Are Shown.

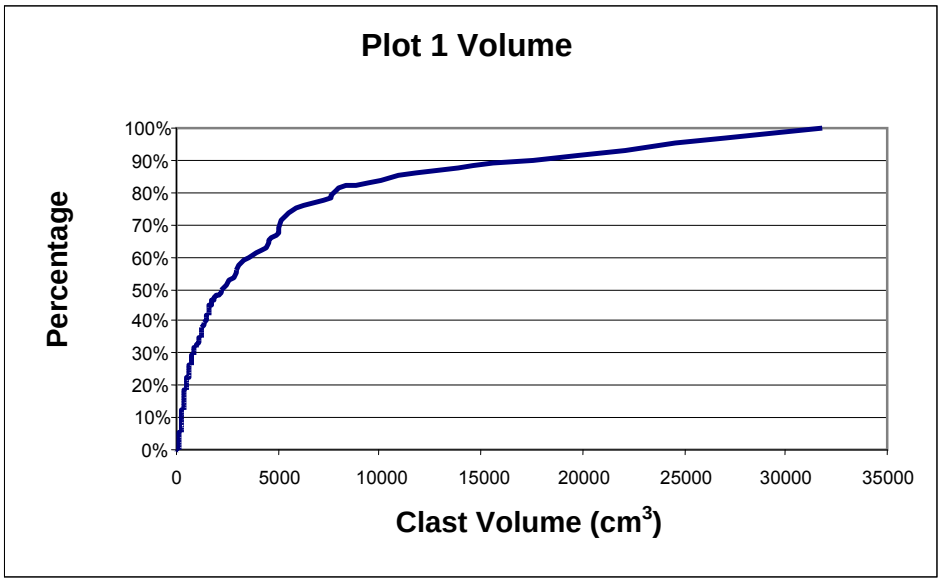

Figure 2-39. Cumulative Frequency Distribution Plot of Rubble Clast Volume From Plot 1

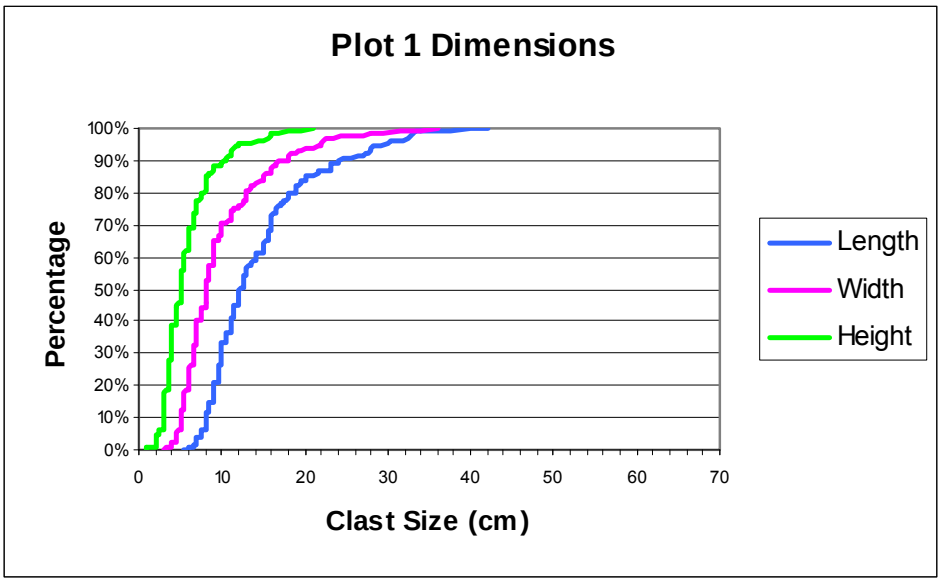

Figure 2-40. Cumulative Frequency Distribution Plot of Rubble Clast Length, Width, and Height From Plot 1

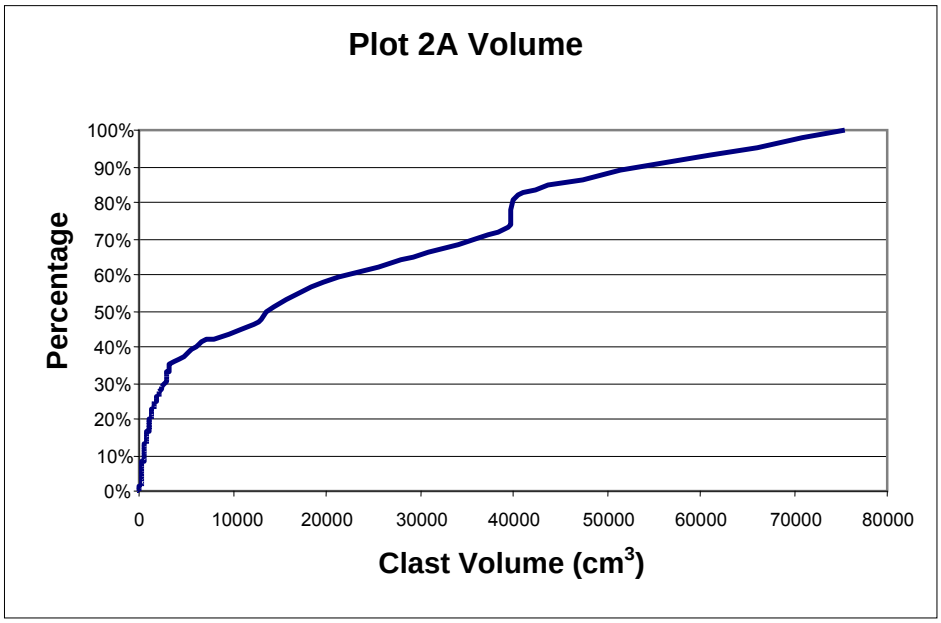

Figure 2-41. Cumulative Frequency Distribution Plot of Rubble Clast Volume From Plot 2A

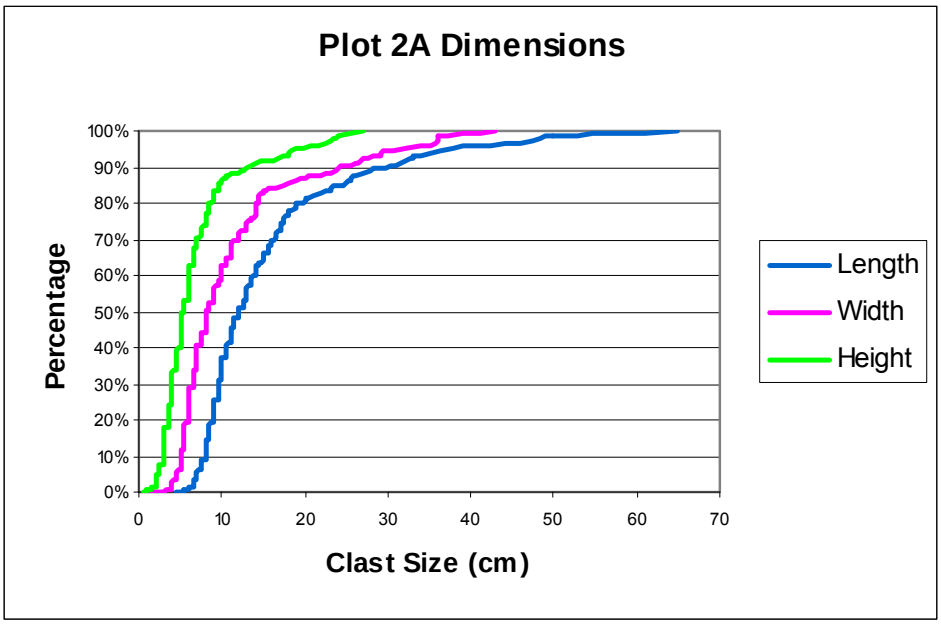

Figure 2-42. Cumulative Frequency Distribution Plot of Rubble Clast Length, Width, and Height From Plot 2A

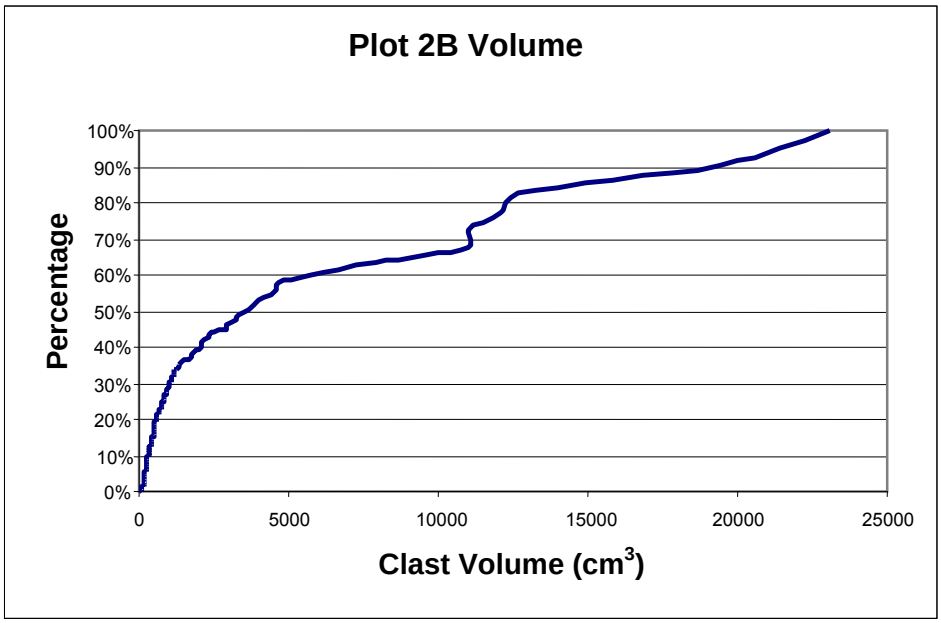

Figure 2-43. Cumulative Frequency Distribution Plot of Rubble Clast Volume From Plot 2B

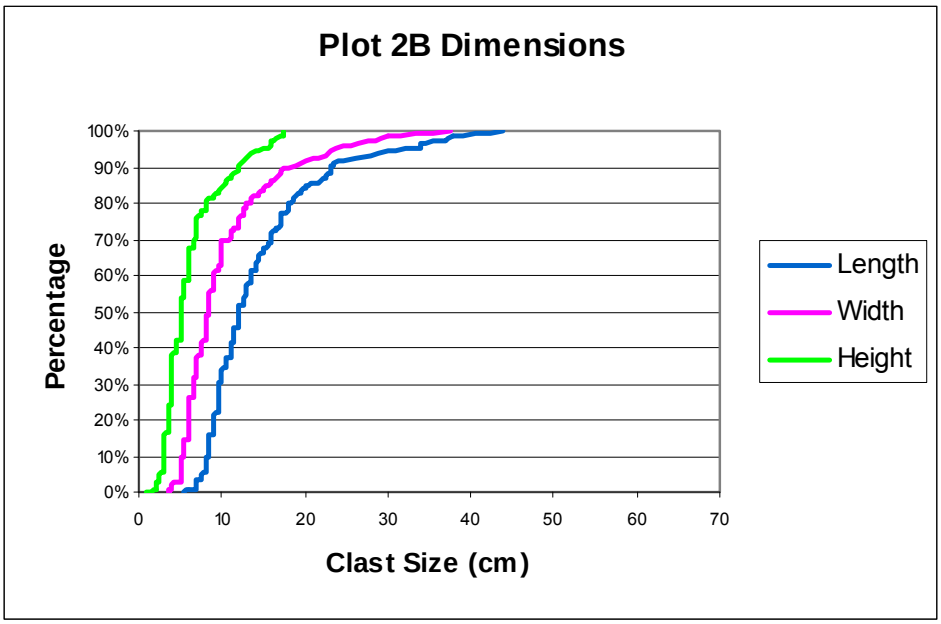

Figure 2-44. Cumulative Frequency Distribution Plot of Rubble Clast Length, Width, and Height From Plot 2B

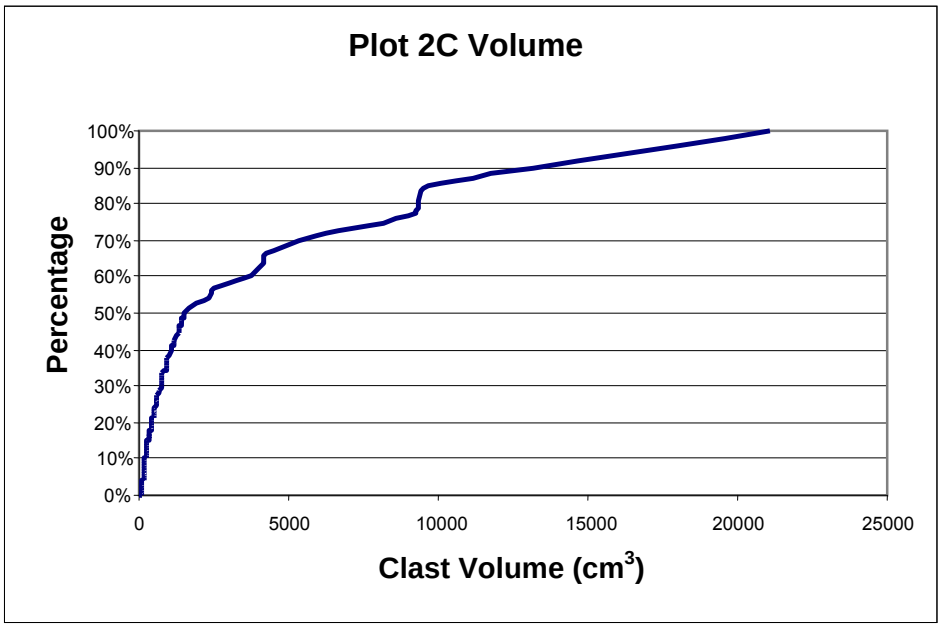

Figure 2-45. Cumulative Frequency Distribution Plot of Rubble Clast Volume From Plot 2C

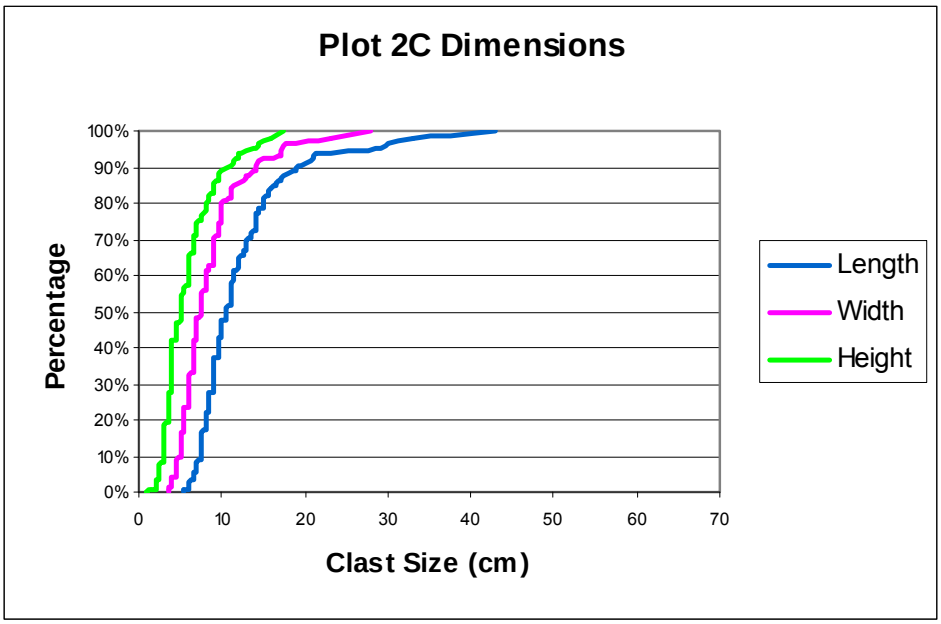

Figure 2-46. Cumulative Frequency Distribution Plot of Rubble Clast Length, Width, and Height From Plot 2C

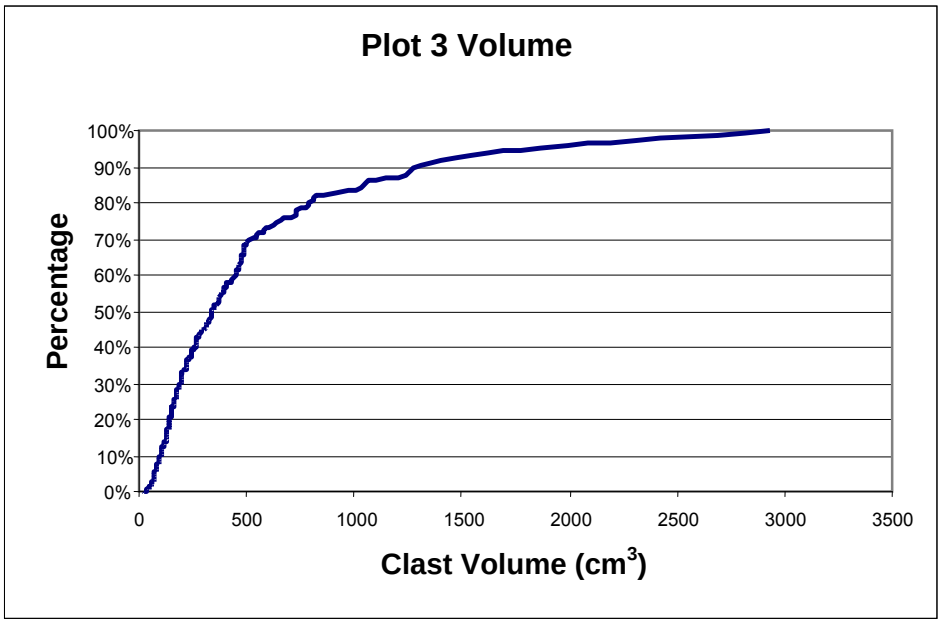

Figure 2-47. Cumulative Frequency Distribution Plot of Rubble Clast Volume From Plot 3

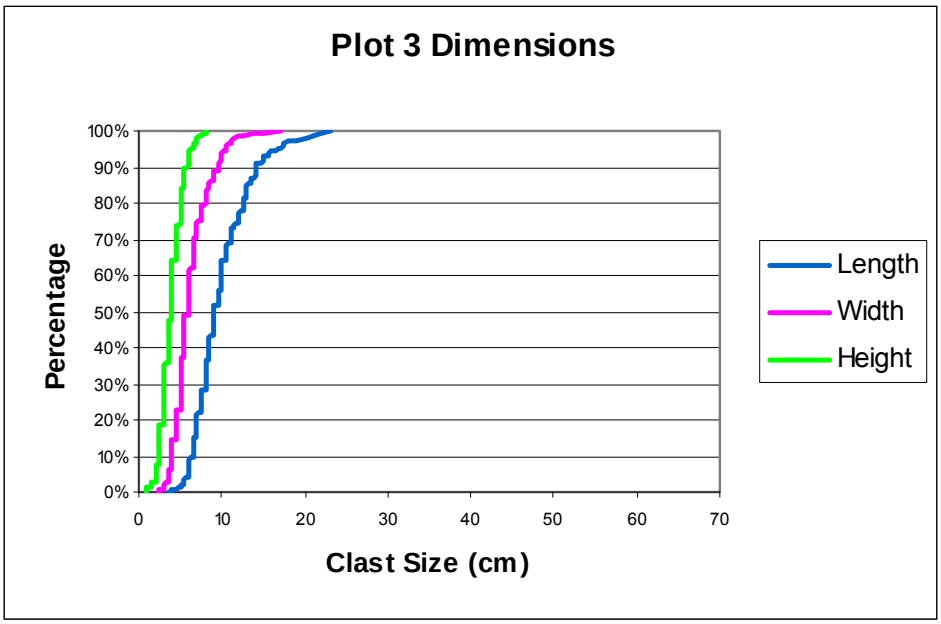

Figure 2-48. Cumulative Frequency Distribution Plot of Rubble Clast Length, Width, and Height From Plot 3

3 LABORATORY MEASUREMENT OF BULKING FACTOR

3.1 Introduction

Rubble obtained from the field investigation at Fran Ridge, described in Section 2, was shipped to the Center for Nuclear Waste Regulatory Analyses (CNWRA®) for further analyses. Planned laboratory tests were expected to provide further information on estimates of possible loose rubble mass densities (bulk density) that may occur in drifts constructed in the Topopah Spring welded lower lithophysal zone (Tptpll). Rubble from Plot 2 was used in the laboratory tests because of the closer link to *in-situ* rock mass densities compared to Plots 1 and 3. The rubble from Plot 2 was extracted directly from an outcrop with minimal force. The resulting rubble and the small percentage of fines were placed in two 0.2 m^3 [55-gal] drums at the field site. Approximately 0.3 m^3 [10.6 ft^3] of rubble from Plot 2 subareas A and B, which included the void volume between rubble fragments in the drums, was shipped to CNWRA. The mass of rubble needed to fill wooden boxes with known dimensions was measured using a calibrated balance. The laboratory test was based on the procedure of Peele (1961, Section 2.4, Measurement of Bulking Factor).

Results of laboratory packing experiments of the loose rubble are presented using two definitions of bulking factor. From a physical perspective, these definitions are the same. They differ in how the factor can be implemented in geological analyses or performance assessments. The two definitions of bulking factor are $\boldsymbol{V_B/V}$ or $\boldsymbol{V_B/V - 1}$, where V_B is the volume taken up by rubble and V is the volume taken up by intact rock. Because the mass of rock remains the same, the ratio of intact bulk density to rubble bulk density is the same as the ratio of the corresponding volumes. The volume increase is reflected as a porosity increase, which leads to increased permeability and decreased thermal conductivity for the rubble compared to that of the intact rock. Permeability and thermal conductivity of the rubble are not estimated as part of this report. An approach for estimating permeability and thermal conductivity using bulking factors and fracture data is described in Mohanty, et al. (2006).

3.2 Bulk Density of Rubble

Two wooden boxes were constructed to determine the mass density of loose rubble (Figure 3-1). The volume of each box was approximately 0.23 m^3 [8.1 ft^3], and each could hold approximately 75 percent of the Plot 2 rubble sample sent to CNWRA. The box volume was chosen to minimize boundary effects associated with the box walls and so that different rubble fragments could be used in replicate packing of the boxes to investigate variability of the measurements. One box (Container 1) was 61.0 cm [2.0 ft] high by 61.0 cm [2.0 ft] wide by 61.0 cm [2.0 ft] long and was cubic in shape. The other box (Container 2) was 61.0 cm [2.0 ft] high by 40.5 cm [1.325 ft] wide by 91.5 cm [3.0 ft] long and was rectangular in shape. The different shaped boxes have slightly different surface area to volume ratios, which could potentially affect measured loose rubble mass density. Much larger boxes, which would further minimize box boundary effects, could not be constructed, because of the limited available rubble volume. Given the rubble size distribution for Plot 2, subareas A and B (Figure 2-1), approximately 10 rubble fragments could fit in each direction within the boxes, except for possibly the shorter dimension of the rectangular box. Figure 3-1(B) shows one packing of the cubic box; the box dimensions are such that approximately 10 rubble fragments can fit into the box dimensions in each direction, which is a generally accepted approach for measuring mass per volume relationships of particles.

Before packing the boxes, all rubble from Plot 2 was removed from the drums and placed on a tarp according to size. When packing the boxes, staff tried to reproduce the size distribution of rubble observed on the tarp in the packed boxes using visual determination. Two box-packing approaches were used to obtain a range of loose rubble mass densities. In some packings, the open spaces between large rubble fragments were not filled with smaller rubble fragments. In other packings, smaller rubble fragments were placed in the larger openings to obtain a denser packing. In all packings, staff adjusted the orientation of the rubble fragments along the box walls to minimize boundary effects.

In packings 1–4, there was no attempt to fill all larger openings between the rubble fragments with smaller sized rubble fragments. However, the packings were conducted such that no extraordinarily large openings or void spaces existed in the packed rubble. There was no attempt to pack the boxes as tightly or densely as possible. In packings 5–7, smaller sized rubble fragments were placed in larger openings/voids between the rubble fragments to produce a denser packing than in packings 1–4. A greater percentage of smaller fragments was used in packings 5–7 than what was observed on the tarp initially and was contained in packings 1–4. Openings/voids remained between the rubble fragments, however, but their size was not as large as may have existed in packings 1–4. The shape of the boxes did not appear to affect the measured, packed rubble mass density.

The loose rubble bulk densities measured in packings 1–7 are shown in Table 3-1. The bulking factors were estimated based on an *in-situ* rock density of 1,979 kg/m^3 [123.5 lb/ft^3] (Bechtel SAIC Company, LLC, 2003) for the Tptpll unit at Yucca Mountain, Nevada. A dry *in-situ* bulk density was used to estimate the bulking factor because the rubble fragments used in determining the rubble bulk densities were dry.

Table 3-1 shows that the packing procedure yielded dissimilar loose rubble densities. Packings 1–4 were less dense than packings 5–7. The bulking factors calculated in Table 3-1 are only estimates. They reflect the bulking factor before any settlement due to load or seismic events. The special care in packing fine particles in larger voids changes the magnitude of the rubble bulk density in a direction similar to increasing static load or shaking by earthquakes; however, no representation of these processes is otherwise implied by the packing method.

(A)

(B)

(C)

Figure 3-1. Experimental Setup To Determine Mass Density of Packed Rubble (A) Container 1—Cubic Shape, (B) Top View of Container 1, and (C) Container 2—Rectangular Shape

Table 3-1. Bulk Density of Rubble From Laboratory Measurements Assuming *In-Situ* (Intact) Bulk Density of 1,979 kg/m^3 [124 lbs]. Definitions of Bulking Factor Use V_B for the Rubble Volume and V for the Intact Rock Volume.					
Packing Number	**Container***	**Total Mass (kg)†**	**Rubble Density (kg/m^3)‡**	**Bulking Factor (-) Using V_B/V Definition**	**Bulking Factor (%) Using V_B/V-1 Definition**
1	1	244.05	1,080	1.83	83
2	2	256.29	1,130	1.75	75
3	1	257.12	1,130	1.75	75
4	2	260.74	1,150	1.72	72
5	1	284.34	1,250	1.58	58
6	2	273.17	1,210	1.64	64
7	1	276.32	1,220	1.62	62

*Volume of Container 1 = 0.23 m^3 [8.1 ft^3]; Volume of Container 2 = 0.226 m^3 [7.98 ft^3]
†1 kg = 2.2 lb
‡1 kg/m^3 = 0.062 lb/ft^3

4 SUMMARY

Field data collected at surface exposures of the Tptpll at the south end of Fran Ridge provide additional information potentially relevant to conditions that could arise in the drifts of a high-level waste repository at Yucca Mountain. In general, the fracture data collected from the Topopah Springs welded lower lithophysal zone at the Fran Ridge outcrop are in good agreement with the fracture data collected in the exploratory drifts. The similarity of the fracture data, both in orientation and spacing, between the Fran Ridge outcrop and the small-scale fracture data in the ECRB lends confidence that the fracture and rubble clast data collected are of a comparable range. As observed in the field, rubble shape and size are strongly controlled by the fracture characteristics. The three primary fracture set orientations appear to contribute to the majority of rubble clasts being bladed or elongate in shape. At the drift scale, clast shape distribution is expected to remain consistent with the outcrop data because the fracture orientation data (the primary control on shape) are similar. Particle shape is an important component in determining bulking factor, with more angular fragments contributing to a higher bulking factor. The relationship between fracture spacing and rubble size distribution can be seen in the fracture/rubble characteristics of Plot 3 versus Plots 1 and 2. Rubble size distribution curves provide the range of particle sizes in the outcrop data and may help define appropriate size gradation estimates at the drift scale. The field data collection could not quantify the smallest particle sizes {>0.5 cm [0.20 in] fine-grained material} that may have been transported into or eroded away from the outcrop. The percentage of fines in a rubble pile will affect bulking factor, with a higher percentage producing a lower bulking factor. The supplementary information from the outcrop characterization, combined with knowledge from other sources (e.g., fracture analyses; Smart et al., 2006), may be used to further refine or constrain bulking factor estimates. Rock fragments from the field site were repacked in known volumes to estimate a rubble bulk density. Using a range of packing approaches, estimates of bulking factor ranged between 1.62 and 1.83. These values represent early time rubble piles, or the upper end of the range of long-term rubble piles that have experienced increased static loads and shaking by earthquakes.

5 REFERENCES

Bechtel SAIC Company, LLC. "Subsurface Geotechnical Parameters." Report 800–K0C–WIS0–00400–000–00A. Las Vegas, Nevada: Bechtel SAIC Company, LLC. 2003.

Day, W.C., R.P. Dickerson, C.J. Potter, D.S. Sweetkind, C.A. San Juan, R.M Drake II, and C.J. Fridrich. "Bedrock Geologic Map of the Yucca Mountain Area, Nye County, Nevada." U.S. Geological Survey Geologic Investigations Series I-2627. 1998.

Graham, D.J. and N.G. Midgley. "Graphical Representation of Particle Shape Using Triangular Diagrams." *Earth Surface Processes and Landforms.* Vol. 25. pp. 1,473–1,477. 2000.

Mohanty, S., A. Ghosh, and G. Adams. "Heat Transfer by Natural Convection Through Rubble Generated by Drift Degradation." Proceedings Paper in the International High Level Radioactive Waste Management Conference, Las Vegas, Nevada, April 30–May 4, 2006. La Grange Park, Illinois: American Nuclear Society. 2006.

Pappas, D.M. and C. Mark. "Behavior of Simulated Longwall Gob Material." Report of Investigations RI 9458. Washington, DC: U.S. Bureau of Mines. 1993.

Peele, R. *Mining Engineers' Handbook*. 3rd Edition. New York City, New York: John Wiley & Sons. 1961.

Rockware, Inc. "StereoStat Version 1.4." Golden, Colorado: Rockware, Inc. 2004.

Smart, K. and R. Fedors. "Trip Report: Field Examination of Lithophysal Rocks at Yucca Mountain." San Antonio, Texas: CNWRA. 2006.

Smart, K.J., D.Y. Wyrick, P.S. Landis, and D.J. Waiting. "Summary and Analysis of Subsurface Fracture Data from the Topopah Spring Tuff Upper Lithophysal, Middle Nonlithophysal, Lower Lithophysal, and Lower Nonlithophysal Zones at Yucca Mountain, Nevada." CNWRA 2005-04. ML060660009. San Antonio, Texas: CNWRA. 2006.

Sneed, E.D. and R.L. Folk. "Pebbles in The Lower Colorado River, Texas, A Study of Particle Morphogenesis. *Journal of Geology.* Vol. 66, No. 2. pp. 114–150. 1958.

Wyrick, D., R. Fedors, K. Smart, and R. McGinnis. "Trip Report: Field Examination of Fractures and Talus From Lithophysal Tuffs at a Rubble Analog Site, South End of Fran Ridge, Yucca Mountain, Nevada, February 5–8, 2007." San Antonio, Texas: CNWRA. 2007.